The origin of the ice-free areas of the Hurd Peninsula (Livingston Island, Antarctica)

Marc Oliva, David Palacios, Leopoldo G. Sancho, José M. Fernández-Fernández, Attila Çiner, Marcelo Fernandes, Julia García-Oteyza, M. Akif Sarıkaya, Enrique Serrano, Amaneh Kaveh-Firouz, et al.

Quaternary Science Reviews 344 (2024) 108991

Contents lists available at ScienceDirect

Quaternary Science Reviews

journal homepage: www.elsevier.com/locate/quascirev

The origin of the ice-free areas of the Hurd Peninsula (Livingston Island, Antarctica)

Marc Oliva [a,*], David Palacios [b], Leopoldo G. Sancho [c], José M. Fernández-Fernández [b], Attila Çiner [d], Marcelo Fernandes [e], Julia García-Oteyza [a], M. Akif Sarıkaya [d], Enrique Serrano [f], Amaneh Kaveh-Firouz [d,g], Augusto Pérez-Alberti [h], Irene Schimmelpfennig [i], Gonçalo Vieira [e], Josep Bonsoms [a], Dermot Antoniades [j], ASTER Team [i,1]

[a] Department of Geography, Universitat de Barcelona, Spain
[b] Department of Geography, Universidad Complutense de Madrid, Spain
[c] Department of Pharmacology, Pharmacognosy and Botany, Universidad Complutense de Madrid, Spain
[d] Eurasia Institute of Earth Sciences, Istanbul Technical University, Turkiye
[e] Centre for Geographical Studies, Associate Laboratory Terra, IGOT, University of Lisbon, Portugal
[f] Department of Geography, Universidad de Valladolid, Spain
[g] Institute of Tibetan Plateau Research, Chinese Academy of Sciences, Beijing, China
[h] Department of Soil Science and Agricultural Chemistry. Universidade de Santiago Compostela, Spain
[i] Aix-Marseille Université, CNRS, IRD, INRAE, UM 34 CEREGE, Aix-en-Provence, France
[j] Department of Geography and Centre for Northern Studies, Université Laval, Canada

ARTICLE INFO

Keywords:
Geomorphology
Antarctica
South shetland islands
Hurd peninsula
Deglaciation
Cosmic-ray exposure ^{10}Be dating
Lichenometry

ABSTRACT

Spatio-temporal patterns of glacial retreat determine the intensity of geomorphological, hydrological, and ecological processes in the ice-free areas of the Antarctic Peninsula region. The chronology of glacial oscillations in the region following the Last Glacial Maximum (LGM) is still poorly constrained and mostly limited to data from a few sites adjacent to research stations. The Hurd Peninsula, located on Livingston Island (South Shetland Islands), is mainly covered by the Hurd Peninsula Ice Cap (HPIC); there is a ca. 20 km^2 ice-free area downvalley of the ice cap in the peninsula's southern sector in addition to numerous nunataks that protrude above the HPIC. In this study, we present an approach combining two direct surface exposure dating methods, cosmic-ray exposure (CRE) dating and lichenometry, to reconstruct the spatio-temporal patterns of glacial thinning and ice cap retreat on the Hurd Peninsula. To understand the patterns of deglaciation on the peninsula, 26 samples for CRE dating (*in situ* cosmogenic ^{10}Be) were taken from glacially polished surfaces and moraine boulders along a transect from the nunatak summits to the coast. On the most recent moraines, boulder stabilisation (i.e., indicative of glacier withdrawal) was dated through the longest axis of the 10 largest thalli of the lichen species *Rhizocarpon geographicum*. Ice thinning might have begun before the LGM at ca. 31.6 ka, when the highest areas close to the coast became exposed, and subsequently accelerated during the LGM at 20-18 ka. The upper surfaces were completely deglaciated between 16 and 14 ka. The HPIC was relatively stable until the mid-Holocene, when neoglacial advances of its outlet glaciers built moraines at ca. 4.5 ka. Subsequently, late Holocene polygenic moraines formed before the development of the external ridges of the most recent moraine system left by the HPIC outlets during the Little Ice Age, at 0.3 ka. The internal moraines correspond to glacial advances from the late 19th and early 20th centuries, as indicated by lichenometric dating. This work presents a comprehensive chronology of glacial oscillations on the Hurd Peninsula, enhancing our understanding of deglaciation patterns and offering insights into glacier dynamics due to climate variability and change.

* Corresponding author.
E-mail address: marcoliva@ub.edu (M. Oliva).
[1] Consortium: Georges Aumaître, Karim Keddadouche.

https://doi.org/10.1016/j.quascirev.2024.108991
Received 11 July 2024; Received in revised form 30 September 2024; Accepted 1 October 2024
Available online 20 October 2024

1. Introduction

In the current climate scenario of accelerated warming, reconstruction of past glacier oscillations is particularly important to frame the current pattern of glacier shrinkage within the natural environmental range and to improve our understanding of the sensitivity of glaciers to climate variability. This is particularly relevant in areas such as the northern Antarctic Peninsula, where mean annual temperatures at sea level are close to 0 °C. As glaciers are highly sensitive to fluctuations in temperature and precipitation regimes, increased warming may impact negatively glacier mass balances in the AP, and this region may become an important source of future sea-level rise.

The global climate system during the Quaternary has been strongly influenced by large variations in polar ice accumulation. This accumulation peaked at 26-19 ka, a period known as the global Last Glacial Maximum (LGM), coinciding with the coldest global conditions of the last glacial cycle (Clark et al., 2009). Since then, glaciers have retreated significantly, with readvances and retreats depending on prevailing climate conditions. Changes in ice dynamics were particularly intense during the so-called Termination-1 (19-11 ka; Denton et al., 2010), which caused major environmental changes on a global scale (redefinition of coastlines, permafrost thawing, changes in river dynamics, etc.) as well as a major reorganisation of ocean and atmospheric currents. In contrast to Termination-1, polar ice sheets, ice caps, and mountain glaciers have undergone rather modest changes since the beginning of the Holocene (Briner et al., 2020; Young et al., 2020). However, the accelerated global-scale ice retreat of the past few centuries determined the configuration of the present-day ice-free landscapes (Hall, 2009; O'Cofaigh et al., 2014).

Currently, only 0.4% of Antarctica is ice-free. The Antarctic Peninsula region, which is still 98% glaciated, contains numerous small ice-free areas, mostly along coastal areas and at the highest peaks (Ingólfsson et al., 1998). Some studies have attempted to reconstruct the ice sheet configuration of the Antarctic Peninsula from the LGM to the present (Ó Cofaigh et al., 2014). Previous palaeoenvironmental studies have focused on terrestrial and marine records, mostly using ^{14}C dating, which provides minimum ages indicating the initial development of soils, fauna, and vegetation, often with an unknown lag time after glacial retreat (Oliva et al., 2016a,b; Navas et al., 2017). More recently, cosmic-ray exposure (CRE) dating applied to glacial landforms and deposits has provided new insights into the timing and spatial patterns of land surface exposure in this region during past millennia (Palacios et al., 2020; Fernández-Fernández et al., 2021; Oliva et al., 2024). Other dating techniques, such as optically stimulated luminescence, have also been applied to sedimentological records associated with glacial retreat including lacustrine sediments and raised beaches (Palacios et al., 2020). For more recent timescales, dating approaches such as lichenometry have not been widely used in the Antarctic Peninsula, despite

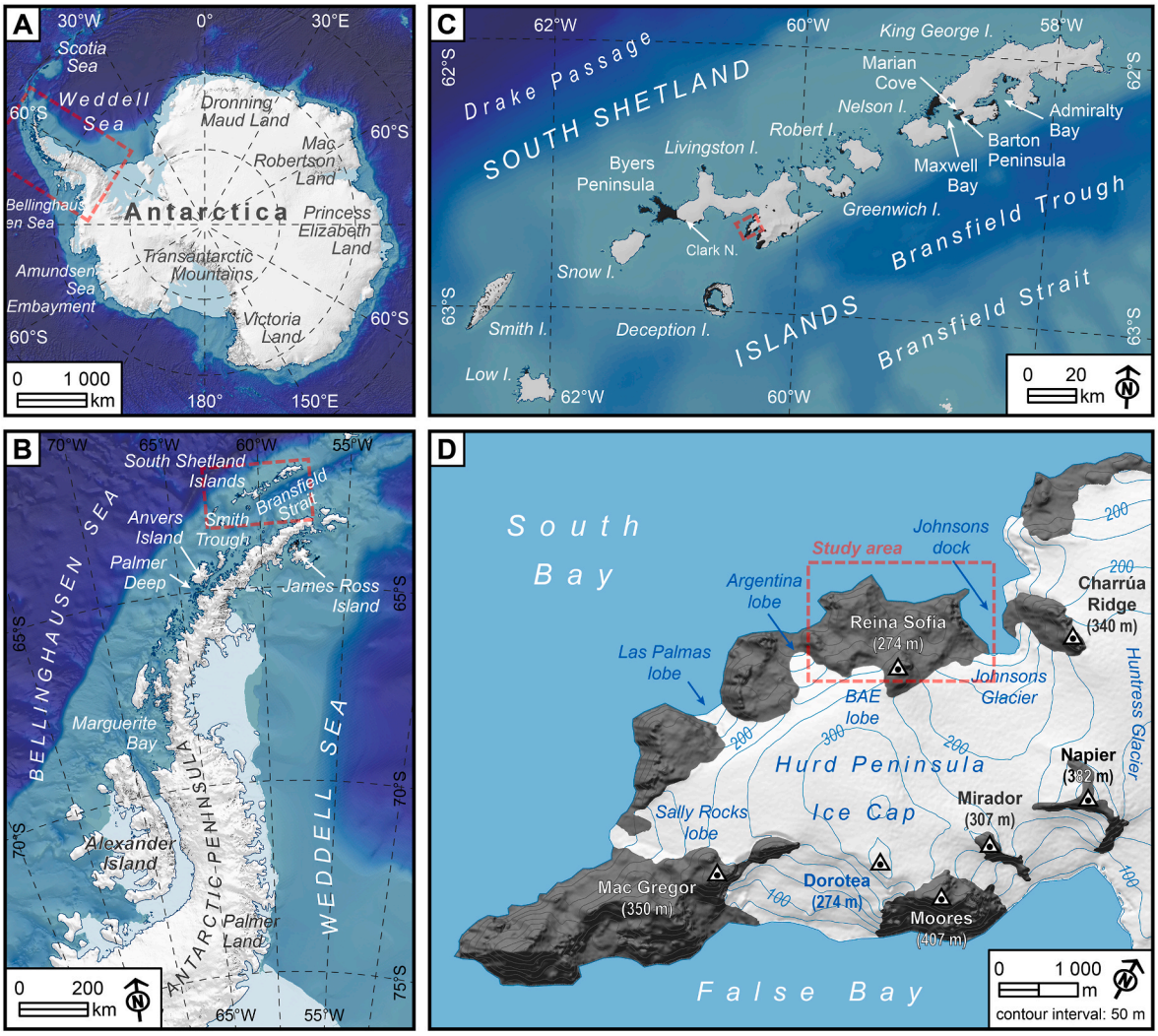

Fig. 1. Location of the study sites within (A) the Antarctic continent, (B) the Antarctic Peninsula, (C) the South Shetland Islands and (D) the Hurd Peninsula. Source: SCAR Antarctic Digital Database (ADD).

age-size curves being available for some locations (Golledge et al., 2010; Sancho et al., 2017). The timing of deglaciation also affects geo-ecological dynamics, favouring permafrost degradation or aggradation, changes in geomorphic and soil processes, plant colonisation, the arrival of fauna, etc. (Ruiz-Fernández et al., 2019).

Several records scattered across the Antarctic Peninsula indicate that glacial thinning began during the LGM. In the South Shetland Islands (SSI; Fig. 1), the focus of this study, Seong et al. (2009) dated the onset of exposure of the highest peaks on the Barton Peninsula (King George Island) to 15.5 ± 2.5 ^{36}Cl ka, recalculated to ca. 16.1 ka based on the latest *in-situ* ^{36}Cl production rates (Fernández-Fernández et al., 2021). Similarly, ice thinning was also underway at other SSI sites between 24 and 22 ka, as inferred from vertical sequences on nunataks, including those on the Byers (Oliva et al., 2019a,b) and Hurd peninsulas (Fernández-Fernández et al., 2021), both on Livingston Island. This thinning, which intensified between ca. 18 and ca. 13 ka, was accompanied by horizontal ice mass retreat, exposing large ice-free areas during the Late Glacial and Early Holocene. The deglaciation process accelerated at ca. 8 ka and created the largest ice-free areas that exist today in the SSI, as revealed by CRE dating of glacial landforms and ^{14}C dating of lake sediments from the Fildes, Barton and Potter peninsulas on King George Island (Giralt et al., 2020; Heredia-Barión, 2019, 2023; Oliva et al., 2019a), as well as from Byers Peninsula in Livingston Island (Oliva et al., 2016a, 2016b). Since the Mid-Holocene, glacial advances in the region appear to have been limited and mainly confined to present-day glacial forelands, such as those documented on the Fildes (Hall, 2007; Oliva et al., 2023) and Byers (Palacios et al., 2020) peninsulas, where glacial advances occurred at ca. 4.5-4.0 and 1 ka have been associated with the Neoglacial period (Porter, 2001). The age of moraines has also been tentatively dated from cross-cutting relationships with dated raised beaches (Hall, 2003; John and Sugden, 1972; Simms et al., 2021). However, the timing of the most recent glacial phases in the SSI has not yet been assessed by direct dating of glacial landforms.

The aim of this study was to investigate the spatio-temporal dynamics of glacier oscillations on the Hurd Peninsula based on the geomorphological record, particularly in the northern limit of the Hurd Peninsula Ice Cap (HPIC; Fig. 1). This peninsula is one of the most visited ice-free areas in the northern Antarctic Peninsula, as it hosts the Spanish 'Juan Carlos I' research station, providing logistical facilities for studies of its terrestrial ecosystem. Therefore, an accurate chronology of glacial retreat and ice-free exposure is crucial as context for better understanding hydrological and geomorphological processes, soil formation, vegetation colonisation, and analysing faunal patterns in the region. The following questions will be addressed.

(i) When did the HPIC begin to retreat from the present ice-free area of the Hurd Peninsula?
(ii) Are there any glacial landforms from the Neoglacial period? If so, how extensive were the Neoglacial oscillations?
(iii) Do the observed chronological patterns fit with larger regional trends in Antarctica?

2. Study area

The SSI are located NW of the Antarctic Peninsula and comprise several extensively glaciated islands (Fig. 1). Livingston Island is the second largest island of the archipelago (ca. 818 km^2), with ca. 85% of its surface covered by mountain glaciers and ice caps. This study focuses on the Hurd Peninsula, a ca. 20 km^2 ice-free area on Livingston Island where the highest summits reach 270–340 m asl.

Climatic conditions on the Hurd Peninsula are typical of a polar maritime regime, with a mean annual air temperature of −2 °C at sea level and precipitation between 500 and 800 mm per year (Bañón et al., 2013). The bedrock consists of a low-grade metamorphic turbidite sequence with alternating layers of quartzite and shale, together with conglomerates and breccias known as the Miers Bluff Formation (Arche et al., 1996; Smellie et al., 1995). The substrate is affected by intense cryogenic processes due to the frequent freeze-thaw cycles typical of polar maritime periglacial environments. Present-day geomorphological dynamics are strongly influenced by permafrost, which is widespread in the SSI along a gradient from continuous above 140–150 m asl (Ferreira et al., 2017) through discontinuous to patchy at lower altitudes (Vieira et al., 2010; Correia et al., 2017; Hrbáček et al., 2020, 2024). Geomorphic features such as moraines, till, erratic boulders, and polished surfaces are widespread, providing evidence that the ice-free area of the Hurd Peninsula has undergone significant glaciation in the recent past (López-Martínez et al., 2012).

The ice-free areas of the Hurd Peninsula are separated by the HPIC, which feeds several outlet glaciers between South Bay and False Bay (Fig. 1). The peninsula's glacial drainage pattern is determined by the distribution of several peaks on its margins, as well as of several nunataks (ca. 300–400 m asl) protruding from the ice cap. These features divide the glacier flow towards the Huntress Glacier (SE) and towards the outlet glaciers on the western HPIC margin: Johnsons Glacier (NW), BAE Glacier (NW; unofficial local name for the Spanish Base Valley lobe), Argentina lobe (NW), Las Palmas (W) and Hurd and Sally Rocks (SW). Some of these are tidewater glaciers, such as Johnsons Glacier, one of the largest glaciers on the peninsula, with a present-day equilibrium-line altitude (ELA) located at 150–180 m asl (Molina et al., 2007), while others, including the BAE Glacier, are land-terminating. As a result of the pronounced warming over the Antarctic Peninsula region during the second half of the 20th century (Turner et al., 2005), the HPIC lost a significant volume of ice (Molina et al., 2007), although a deceleration of this trend has been reported in the early 21st century (Navarro et al., 2013; Osmanoglu et al., 2014) in response to a subsequent cooling trend detected in the Antarctic Peninsula region (Oliva et al., 2017). This trend has now switched back to warming again, setting new all-time records for the instrumental period in 2022 (González-Herrero et al., 2022).

The recent changes in ice volume stored in the HPIC must be seen in the context of long-term thinning in the area since the end of the last glacial cycle (Nývlt et al., 2020). CRE dates from vertical sequences on the ancient nunataks surrounding the plateau suggest that the ice began to thin during the LGM at ca. 22 ka and continued between ca. 18 and 13 ka, with particularly intense thinning between ca. 14 and 13 ka and relative stability throughout the Holocene (Fernández-Fernández et al., 2021). However, these small volume changes during the Holocene must have favoured significant horizontal ice retreats, exposing the relatively-low current ice-free areas. This pattern has been observed in the westernmost part of Livingston Island (Oliva et al., 2016a,b; Palacios et al., 2020) as well as in other ice-free areas of the SSI (Heredia Barión et al., 2023a, 2023b; Oliva et al., 2019b; Oliva et al., 2016b, 2023).

3. Methodology

Fieldwork was conducted during the austral summers of 2017 and 2018, near the end of the ablation season, in order to best identify the various glacial features in the ice-free areas surrounding the HPIC and to collect samples for CRE dating.

3.1. Sampling strategy

The ice-free areas of Maritime Antarctica are affected by intense periglacial conditions, and bedrock is heavily fractured due to frost shattering. As such, few remnants remain of the original surfaces, and special care must be taken when selecting and sampling target features. We collected 26 samples from well-preserved glacially polished surfaces and stable (well-anchored) moraine boulders of granitoid and quarzitic lithologies (Fig. 2). To ensure optimal exposure to cosmic ray flux, flat or gently sloping (≤26°) surfaces of the rock outcrops were preferred to steep slopes and sharp crests. The thickness of the extracted rock fragments ranged between 1.5 and 5.0 cm (see Table 1).

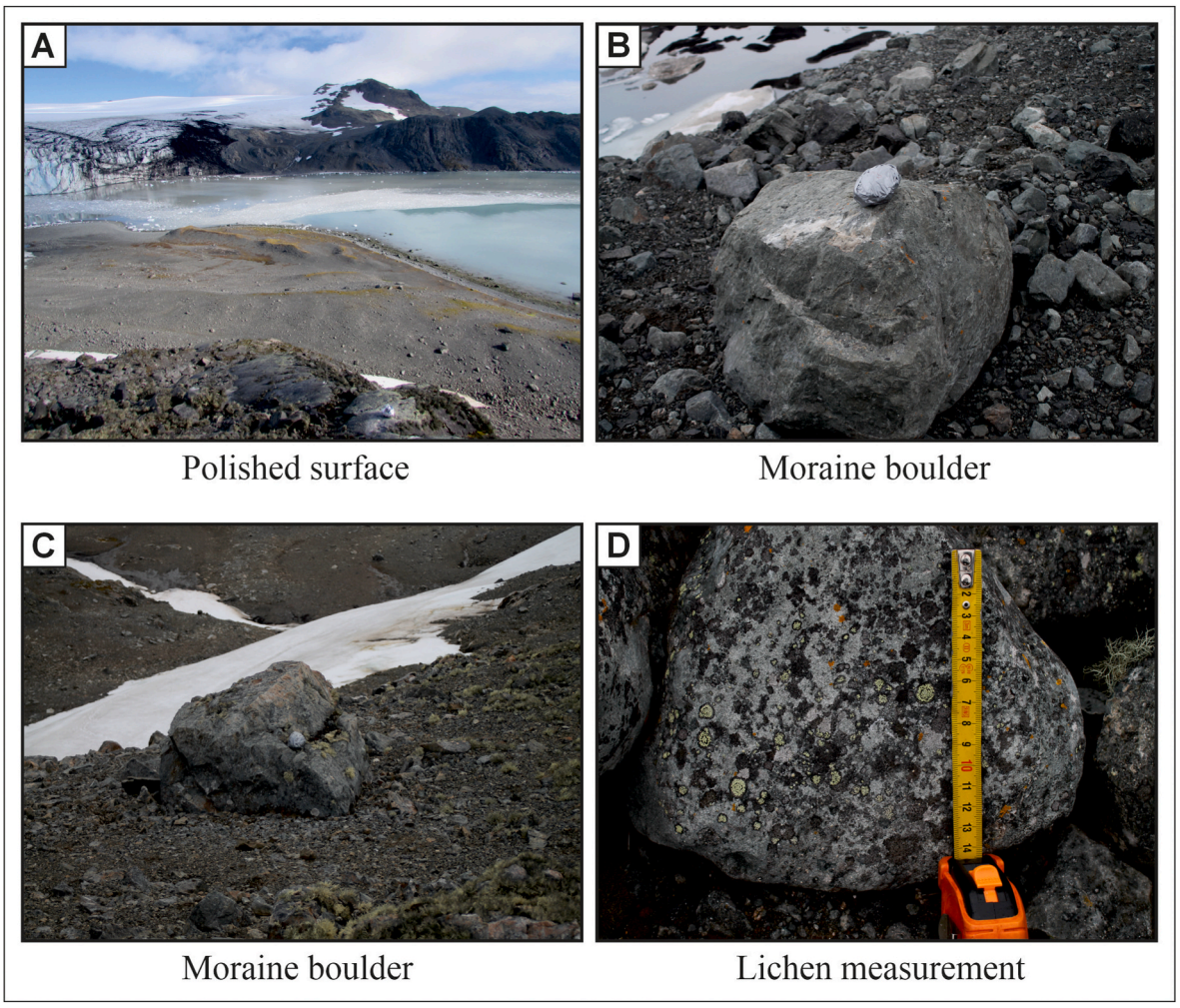

Fig. 2. Examples of different sample sites for CRE ^{10}Be and lichenometric dating.

3.2. Laboratory procedures and exposure age calculation

After field sampling, rock samples were crushed and sieved to the 0.25–1.0 mm fraction in the 'Physical Geography Laboratory' of the Universidad Complutense de Madrid (Madrid, Spain). Due to the quartz-rich lithology of the samples, the *in-situ* produced cosmogenic nuclide ^{10}Be was chosen for surface exposure dating. Quartz isolation was done at ITU/Kozmo-Lab (Istanbul, Türkiye) through a magnetic separation with a 'Frantz LB-1' magnetic barrier separator subsequent to chemical attacks with a concentrated mixture of hydrochloric (1/3 HCl) and hexafluorosilicic (2/3 H_2SiF_6) acids. Decontamination to remove meteoric ^{10}Be was conducted through successive partial dissolutions with concentrated hydrofluoric acid (HF). Further subsequent chemical procedures were conducted at the Laboratoire National des Nucléides Cosmogéniques (LN_2C) of the Centre Européen de Recherche et d'Enseignement des Géosciences de l'Environnement (CEREGE, Aix-en Provence, France). Laboratory procedures followed the protocols outlined in Fernández-Fernández et al. (2021). The purified quartz was then spiked with 150 mL of an in-house manufactured (from a phenakite crystal) ^{9}Be carrier solution (3025 ± 9 mg ^{9}Be g^{-1}; Merchel et al., 2008) and totally dissolved in HF. After total dissolution, Be was isolated from other elements (Fe, Mn, Al) using Dowex® anionic and cationic exchange resin columns (1X8 and 50WX8, respectively; Merchel and Herpers, 1999). Final BeO targets were mixed with niobium powder and loaded on nickel cathodes for further ^{10}Be/^{9}Be ratio measurement at the 'Accelerateur pour les Sciences de la Terre, Environnement et Risques' (ASTER) national AMS facility at CEREGE from which ^{10}Be concentrations were later inferred (Table 3). The AMS measurements were calibrated against the in-house standard STD-11, with an assigned ^{10}Be/^{9}Be ratio of 1.191 ± 0.013 (Braucher et al., 2015). Analytical 1-sigma uncertainties of the AMS measurements include uncertainties in counting statistics, the standard ^{10}Be/^{9}Be ratio, and an external 0.5% AMS error (Arnold et al., 2010). The ^{10}Be half-life used was 1.387 ± 0.0012 × 10^{6} years (Chmeleff et al., 2010; Korschinek et al., 2010). The number of ^{10}Be atoms in the samples was corrected for that in the procedural blank (Table 3). We calculated the ^{10}Be exposure ages with the CRONUS-Earth v 3.0 exposure age online calculator (Balco et al., 2008; available online at https://hess.ess.washington.edu/), which is the most commonly used throughout Antarctica. For the calculations, we used the default global calibration data set, whose reference sea-level high latitude (SLHL) production rate is derived from the primary calibration dataset of Borchers et al. (2016) with calibration through the ICE-D calibration database (http://calibration.ice-d.org/), the single-formula Antarctic atmosphere approximation ('antatm' in the online calculator; Stone, 2000), an assumed quartz density of 2.7 g cm^{-3} and no corrections on surface erosion and snow shielding. The topographic shielding factor was calculated through the Python-based ArcGIS toolbox devised by Li (2018), which only requires a point shapefile with the location of the samples, their associated field data (strike, dip, and height of the sampled surface), and a digital elevation model. The exposure ages according to the 'LSDn' (Lifton et al., 2014) production rate scaling model can be found in Table 3. We used the production rates most commonly applied in studies across Antarctica so that our data would be comparable with other studies of glacier oscillations carried

Table 1
Geographic location of CRE samples, topographic shielding factor and sample thickness.

Sample name	Landform	Latitude (DD)	Longitude (DD)	Elevation (m a.s.l.)[a]	Topographic shielding factor	Thickness (cm)
The Johnsons Glacier						
JO-08	Moraine boulder	−62.6561	−60.3612	105	0.9905	3.7
JO-09	Polished bedrock	−62.6559	−60.3611	105	0.9861	1.8
JO-10	Polished bedrock	−62.6552	−60.3598	135	0.9803	2.9
JO-11	Polished bedrock	−62.6564	−60.3623	66	0.9657	2.3
JO-13	Moraine boulder	−62.6581	−60.3644	7	0.9909	4.0
The BAE Glacier						
Glacier forelands						
BAE-01	Moraine boulder	−62.6695	−60.3865	147	0.9892	4.5
BAE-02	Moraine boulder	−62.6705	−60.3917	169	0.9927	1.5
BAE-03	Moraine boulder	−62.6706	−60.3917	169	0.9895	2.2
High plateaus and ridges						
BAE-04	Moraine boulder	−62.6704	−60.3921	178	0.9963	4.0
BAE-05	Moraine boulder	−62.6704	−60.3921	178	0.9985	3.2
BAE-07	Moraine boulder	−62.6706	−60.3925	179	0.9997	4.0
BAE-08	Moraine boulder	−62.6710	−60.3923	180	0.9992	2.8
BAE-09	Moraine boulder	−62.6710	−60.3923	180	0.9989	3.2
BAE-10	Moraine boulder	−62.6710	−60.3928	181	0.9997	4.0
BAE-11	Polished bedrock	−62.6700	−60.3967	83	0.9813	2.3
BAE-12	Polished bedrock	−62.6713	−60.3972	122	0.9861	3.0
BAE-13	Polished bedrock	−62.6690	−60.3922	150	0.9922	3.0
BAE-14	Polished bedrock	−62.6690	−60.3928	141	0.9957	4.2
BAE-21	Polished bedrock	−62.6679	−60.3820	212	0.9849	4.0
BAE-22	Polished bedrock	−62.6666	−60.3830	148	0.9640	4.5
Mountain slopes and valley floor						
BAE-15	Polished bedrock	−62.6669	−60.3941	119	0.9986	3.0
BAE-16	Polished bedrock	−62.6657	−60.3978	129	0.9997	5.0
BAE-17	Polished bedrock	−62.6646	−60.3940	94	0.9971	3.5
BAE-18	Polished bedrock	−62.6646	−60.3912	47	0.9884	4.5
BAE-19	Moraine boulder	−62.6642	−60.3889	21	0.9915	5.0
BAE-20	Moraine boulder	−62.6641	−60.3889	21	0.9917	4.2

[a] Elevation data were taken from the TanDEM-X and corrected to orthometric by applying the Earth Gravitational Model 2008.

out on the continent and particularly on the Antarctic Peninsula. The ^{10}Be ages presented in the text and figures are given with their external uncertainties, including analytical and production rate uncertainties, while Table 3 shows both external and internal (i.e., only analytical) uncertainties.

During blank correction (i.e., calculation of the number of atoms of ^{10}Be in the blank from the number of atoms of ^{10}Be in the sample) and all other calculations, error propagation was done according to standard methods (Taylor, 1997). As such, the magnitude of the blank correction is reflected in the final uncertainty of the ages and thus gives a measure of their accuracy (reliability). Given the relatively low accuracy (10–20%) of some of our young Holocene (neoglacial) samples, we acknowledge the limitations of our data with respect to high-resolution reconstruction of neoglacial glacier fluctuations, and rather focus on long-term trends that are supported by all samples, independent of the magnitude of blank correction.

3.3. Lichenometric dating

The species *Rhizocarpon geographicum* (L.) DC was chosen for lichenometric measurements, taken with a calliper with an instrumental error of <0.1 mm. As in previous studies, we measured the largest axis (representative of the diameter) of roughly circular crustose thalli. The ten largest thalli in each locality were selected for measurement, and the resulting average was considered to derive the surface exposure ages (Sancho et al., 2017). The experience of 25 years of growth monitoring in several localities in the study area has shown an average talus growth rate of 0.48 mm y^{-1}, although the rate may be as low as 0.35 mm y^{-1} in occasional years with persistent snow cover (Sancho et al., 2017). As we aimed to approximate the ages of the moraines as reliably as possible, we used the mean growth rate to calculate the ages (0.48 mm y^{-1}). We also include ages derived from the lowest possible growth rate as an indication of the degree of uncertainty of the method (Table 2). We note that the lower rate of 0.35 mm yr^{-1} observed in periods of longer snow duration may have been more frequent prior to the last 25 years, which is especially relevant for the older moraines. While other lichens may differ, but *Rhizocarpon* behaves like the annual rings of a regularly growing tree (e.g., holm oak). There is no evidence that *Rh. geographicum*'s growth curve is exponential, but rather the opposite (Armstrong, 2013) and in the species there is no significant relationship between photosynthetic rates and stem size (Raggio et al., 2018). Team members who participated in the field surveys, data processing and interpretation of the results have also participated in studies that applied lichenometric dating to several exposed surfaces of known age (Sancho et al., 2011) that confirmed the linear relationship between age and diameter. As such, we are confident that the growth rates we applied in our study are reliable.

While the ecesis value of *Rh. geographicum* is unknown in the study area, this value varies proportionally to the annual growth rate of its talus (McCarthy and Luckman, 1993). As such, we applied the ecesis value of 15–20 years established in northern Iceland, where *Rh. geographicum* has a very similar growth rate (0.44 mm yr^{-1}; Fernández-Fernández et al., 2019). We have estimated the uncertainty of each age/date from the standard deviation of the 10 largest thalli measured in each location (Table 2).

To avoid the replacement of natural lichen communities, only the innermost moraines of the BAE Glacier were used for lichenometry. The first site was established on the moraine closest to the glacier (BAE-LICHEN-01), a small moraine surrounding the front of the glacier lobe. The BAE Glacier was previously attached to this moraine, but its front has retreated in recent decades and a small lagoon now separates them. The second site (BAE-LICHEN-02) was on a much larger moraine comprising a series of overlapping ridges, located further away from the glacier front. We sampled on the most recent ridge of the group (i.e., the one closest to the glacier), which lies below the moraine ridge where the ^{10}Be samples BAE-01 and BAE-02 were taken.

Table 2
AMS analytical data and calculated exposure ages. $^{10}Be/^{9}Be$ ratios were inferred from measurements at the ASTER AMS facility. No corrections of erosion and snow cover have been made.

^{10}Be samples analytical AMS data							^{10}Be exposure ages (ka)
Sample name	Quartz weight (g)	mass of carrier (^{9}Be mg)	ASTER AMS cathode number	$^{10}Be/^{9}Be$ (10^{-14})	Blank correction (%)	[^{10}Be] (10^{4} atoms g^{-1})	'LSDn' scaling scheme (age ± ext. (int.))
The Johnsons Glacier							
JO-10	40.1319	0.45859	IJBB	10.395 ± 0.406	0.97	7.86 ± 3.11	13.1 ± 0.9 (0.5)
JO-09	53.0186	0.46131	IJBA	11.521 ± 0.391	0.87	6.64 ± 2.28	11.3 ± 0.8 (0.4)
JO-08	59.5167	0.46313	IJAZ	8.119 ± 0.583	1.22	4.17 ± 3.04	7.2 ± 0.7 (0.5)
JO-11	45.8348	0.46010	IJBC	0.931 ± 0.195	10.75	0.56 ± 1.31	1.0 ± 0.2 (0.2)
JO-13	38.6606	0.46071	IJBD	0.607 ± 0.112	16.47	0.40 ± 0.09	0.7 ± 0.2 (0.2)
The BAE Glacier							
Glacier forelands							
BAE-01	5.3598	0.45950	IJBF	0.304 ± 0.03	33.01	1.16 ± 2.08	1.9 ± 0.4 (0.3)
BAE-02	9.6661	0.46010	IJBG	0.188 ± 0.029	53.25	0.28 ± 1.15	0.5 ± 0.2 (0.2)
BAE-03	5.8737	0.46192	IJBH	0.128 ± 0.024	77.96	0.15 ± 1.67	0.3 ± 0.3 (0.3)
High plateaus and ridges							
BAE-21	9.5183	0.46313	IJBY	4.113 ± 0.146	2.42	1.30 ± 4.79	20.2 ± 1.4 (0.7)
BAE-11	10.9263	0.46222	IJBO	3.034 ± 0.141	3.28	8.30 ± 4.02	14.5 ± 1.1 (0.7)
BAE-12	11.9336	0.46888	IJBP	2.844 ± 0.098	3.45	7.21 ± 2.64	12.1 ± 0.8 (0.4)
BAE-22	4.0815	0.46252	IJBZ	0.635 ± 0.057	15.69	4.05 ± 4.57	6.9 ± 0.9 (0.8)
BAE-08	15.912	0.46343	IJBL	2.052 ± 0.11	4.84	3.80 ± 2.19	6.0 ± 0.5 (0.3)
BAE-05	4.1669	0.46373	IJBJ	0.514 ± 0.046	19.32	2.25 ± 1.36	4.9 ± 0.7 (0.6)
BAE-13	19.3927	0.46010	IJBQ	1.867 ± 0.09	5.36	2.80 ± 1.47	4.6 ± 0.4 (0.2)
BAE-14	16.7985	0.46041	IJBS	6.128 ± 0.191	1.63	2.72 ± 2.26	4.5 ± 0.5 (0.4)
BAE-04	20.967	0.45950	IJBI	1.637 ± 0.091	6.12	2.25 ± 1.36	3.6 ± 0.3 (0.2)
BAE-10	8.5270	0.46192	IJBN	0.533 ± 0.045	18.72	1.57 ± 1.79	2.4 ± 0.3 (0.3)
BAE-09	10.598	0.46283	IJBM	0.522 ± 0.044	19.06	1.23 ± 1.42	1.9 ± 0.2 (0.2)
BAE-07	7.3389	0.46192	IJBK	0.316 ± 0.041	31.51	3.08 ± 3.75	1.4 ± 0.3 (0.3)
Mountain slopes and valley floor							
BAE-16	17.2830	0.46131	IJBT	10.684 ± 0.371	0.93	18.9 ± 6.64	31.8 ± 2.2 (1.1)
BAE-15	7.1907	0.46494	IJBR	0.728 ± 0.048	13.60	11.0 ± 3.51	18.4 ± 1.2 (0.6)
BAE-17	5.1602	0.46494	IJBU	1.627 ± 0.084	6.09	9.20 ± 5.21	16.0 ± 1.3 (0.9)
BAE-18	12.3573	0.45950	IJBV	2.565 ± 0.102	3.91	6.13 ± 2.59	11.3 ± 0.8 (0.5)
BAE-20	8.7485	0.46010	IJBX	1.295 ± 0.065	7.73	4.20 ± 2.39	7.8 ± 0.6 (0.4)
BAE-19	7.1340	0.46010	IJBW	1.02 ± 0.062	9.81	3.97 ± 2.81	7.5 ± 0.7 (0.5)
Chemistry blank details							
Blank name	mass of carrier (^{9}Be mg)	ASTER AMS cathode number	$^{10}Be/^{9}Be$ (10^{-14})	[^{10}Be] (10^{4} atoms)			
BL-2	0.1122	IJBE	0.136 ± 0.028	3.077 ± 0.643	–	–	

4. Results

4.1. Geomorphological setting of the samples

The distribution of the main glacial features on the Hurd Peninsula is shown in Fig. 3. Glacially polished surfaces, erratic boulders, and moraine systems are widespread and reveal a complex sequence of changes in glacier extents on the peninsula that resulted from fluctuations in the volume of the HPIC.

4.1.1. The Johnsons Glacier

This study study area is located in the northern sector near Johnsons Dock (Fig. 3) on the SW slope of Charrúa Peak (62°39′23″S 60°20′54″W, 333 m asl). Here, glacial landforms such as moraines and ice-moulded surfaces are well preserved. Johnsons Glacier left a series of frontal moraines in the vicinity of its current snout, as well as other lateral moraines in higher sectors. Two boulders were sampled, on the innermost frontal moraine (close to the glacier front) and the highest moraine remnant deposited on a rock step (JO-13 and JO-11, respectively). Three further CRE samples were collected from well-preserved polished surfaces on three rock steps at different altitudes to reconstruct the ice thinning sequence (JO-08, JO-09, and JO-10; Table 1).

4.1.2. The BAE glacier

To the SE of Johnsons Bay, Spanish Base Valley is a deglaciated valley that reaches the sea and becomes Spanish Cove. The head of the valley is occupied by a ca. 300 m-long outlet lobe (BAE Glacier) emitted from the HPIC that surrounds the NW flank of the Reina Sofia Peak (273 m asl) (Fig. 3). Three main geomorphological units were identified in Spanish Base Valley.

- Mountain slopes and valley floor.

The valley slopes gradually descend from the upper ridges to the open bay, with a sequence of raised beaches in the lowest areas (Spanish Cove). Several glacially polished surfaces at different elevations and with clear traces of glacial abrasion reveal the deglaciation of this sector of the Hurd Peninsula. To reconstruct the history of ice thinning, we sampled a transect from the summit surfaces down to the valley floor (Table 1), where the Spanish Antarctic research station 'Juan Carlos I' is located. On the NW margin of the valley, the highest sample (BAE-16) was collected from the top of Radio Peak, followed by others at lower elevations, including 120 m asl (BAE-15), 93 m asl (BAE-17) and 47 m asl (BAE-18). Finally, two moraine boulders (BAE-19, BAE-20) were sampled near the research station to complete the deglaciation history of the valley bottom.

- High plateaus and ridges.

This unit includes the relatively flat areas below the glacial cirque that form the headwaters of Spanish Base Valley, as well as the upper ridges (130–150 m asl) that connect with Reina Sofia and Radio peaks. To the west of BAE Glacier, just below the outer moraine, a gentle slope culminating in an unnamed hill (192 m asl) separates the valley shaped

Table 3
AMS analytical data and calculated exposure ages. 10Be/9Be ratios were inferred from measurements at the ASTER AMS facility. No corrections of erosion and snow cover have been made.

^{10}Be samples analytical AMS data							^{10}Be exposure ages (ka)
Sample name	Quartz weight (g)	mass of carrier (^{9}Be mg)	ASTER AMS cathode number	^{10}Be/^{9}Be (10^{-14})	Blank correction (%)	[^{10}Be] (10^{4} atoms g^{-1})	LSDn' scaling scheme (age ± ext. err. (int. err.)
The Johnsons Glacier							
JO-10	40.1319	0.45859	IJBB	10.395 ± 0.406	0.97	7.861 ± 0.311	13.1 ± 0.9 (0.5)
JO-09	53.0186	0.46131	IJBA	11.521 ± 0.391	0.87	6.64 ± 0.228	11.3 ± 0.8 (0.4)
JO-08	59.5167	0.46313	IJAZ	8.119 ± 0.583	1.22	4.17 ± 0.304	7.2 ± 0.7 (0.5)
JO-11	45.8348	0.46010	IJBC	0.931 ± 0.195	10.74	0.558 ± 0.131	1.0 ± 0.2 (0.2)
JO-13	38.6606	0.46071	IJBD	0.607 ± 0.112	16.47	0.404 ± 0.09	0.7 ± 0.2 (0.2)
The BAE Glacier							
Glacier forelands							
BAE-01	5.3598	0.45950	IJBF	0.304 ± 0.03	33.01	1.165 ± 0.208	1.9 ± 0.4 (0.3)
BAE-02	9.6661	0.46010	IJBG	0.188 ± 0.029	53.25	0.279 ± 0.115	0.4 ± 0.2 (0.2)
BAE-03	5.8737	0.46192	IJBH	0.128 ± 0.024	77.96	0.148 ± 0.167	0.2 ± 0.3 (0.3)
High plateaus and ridges							
BAE-21	9.5183	0.46313	IJBY	4.113 ± 0.146	2.42	13.048 ± 0.479	20.2 ± 1.4 (0.7)
BAE-11	10.9263	0.46222	IJBO	3.034 ± 0.141	3.28	8.296 ± 0.402	14.5 ± 1.1 (0.7)
BAE-12	11.9336	0.46888	IJBP	2.844 ± 0.098	3.45	7.21 ± 0.264	12.1 ± 0.8 (0.4)
BAE-22	4.0815	0.46252	IJBZ	0.635 ± 0.057	15.69	4.052 ± 0.457	6.9 ± 0.9 (0.8)
BAE-08	15.9116	0.46343	IJBL	2.052 ± 0.11	4.84	3.801 ± 0.219	6.0 ± 0.5 (0.3)
BAE-05	4.1669	0.46373	IJBJ	0.514 ± 0.046	19.32	3.084 ± 0.375	4.9 ± 0.7 (0.6)
BAE-13	19.3927	0.46010	IJBQ	1.867 ± 0.09	5.36	2.801 ± 0.147	4.6 ± 0.4 (0.2)
BAE-14	7.1907	0.46494	IJBR	0.728 ± 0.048	13.60	2.717 ± 0.226	4.5 ± 0.5 (0.4)
BAE-04	20.9672	0.45950	IJBI	1.637 ± 0.091	6.12	2.251 ± 0.136	3.6 ± 0.3 (0.2)
BAE-10	8.5270	0.46192	IJBN	0.533 ± 0.045	18.72	1.567 ± 0.178	2.4 ± 0.3 (0.3)
BAE-09	10.5975	0.46283	IJBM	0.522 ± 0.044	19.06	1.233 ± 0.142	1.9 ± 0.2 (0.2)
BAE-07	7.3389	0.46192	IJBK	0.316 ± 0.041	31.51	0.911 ± 0.194	1.4 ± 0.3 (0.3)
Mountain slopes and valley floor							
BAE-16	17.2830	0.46131	IJBT	10.684 ± 0.371	0.93	18.877 ± 0.664	31.8 ± 2.2 (1.1)
BAE-15	16.7985	0.46041	IJBS	6.128 ± 0.191	1.63	11.039 ± 0.351	18.4 ± 1.2 (0.6)
BAE-17	5.1602	0.46494	IJBU	1.627 ± 0.084	6.08	9.202 ± 0.521	15.9 ± 1.3 (0.9)
BAE-18	12.3573	0.45950	IJBV	2.565 ± 0.102	3.91	6.125 ± 0.259	11.3 ± 0.8 (0.5)
BAE-20	8.7485	0.46010	IJBX	1.295 ± 0.065	7.73	4.2 ± 0.239	7.8 ± 0.6 (0.4)
BAE-19	7.1340	0.46010	IJBW	1.02 ± 0.062	9.81	3.966 ± 0.281	7.5 ± 0.7 (0.5)
Chemistry blank details							
Blank name		mass of carrier (^{9}Be mg)	ASTER AMS cathode number	^{10}Be/^{9}Be (10^{-14})	[^{10}Be] (10^{4} atoms)		
BL-2	.	0.33941	IJBE	0.136 ± 0.028	3.077 ± 0.643	–	–

by the BAE Glacier from the adjacent valley to the west moulded by the Argentina Glacier. Surrounding the unnamed hill, there are several well-anchored moraine boulders about 140 m from the present snout, six of which were sampled for CRE dating (BAE-04, BAE-05, BAE-07, BAE-08, BAE-09, BAE-10). Due to their similar altitude and arrangement (see Table 1), they are considered part of the same geomorphological system. Downslope, the glacial valley associated with the BAE Glacier descends towards the sea and includes other moraine systems and widespread glacially polished surfaces. Ca. 240 m from the present glacier terminus, there is a moraine remnant where stable boulders were sampled for CRE dating (BAE-13, BAE-14). On the western slope of the unnamed hill, two polished and striated glacial surfaces were sampled ca. 400 and 300 m from the current glacier terminus (BAE-12 and BAE-11, respectively). On the N-NE side of the valley, on the western slope of Reina Sofia Peak facing Spanish Base Valley, two samples were also taken from polished surfaces (BAE-21, BAE-22).

- Glacier forelands.

This geomorphological unit includes the most recent moraine system left by the BAE Glacier, composed of two main ridges. The innermost moraine with two minor ridges (moraine 1 and 2) is located about 50 m from the present snout and was surveyed for lichenometric dating purposes. At a 50–100 m distance and separated by a proglacial lake, three samples (BAE-01; BAE-02 and BAE-03) were collected on the external (and larger) moraine ridge.

4.2. CRE results

The chronological framework derived from the 26 CRE dates obtained from glacial features distributed across the peninsula spans the period from the LGM to the last several centuries (Fig. 4).

4.2.1. The Johnsons Glacier

The CRE results follow a sequential chronological spatial pattern (Table 3) according to their relative position (elevation) and arrangement in the study area. The highest moraine boulder yielded 7.2 ± 0.7 ka (JO-08), and the polished surfaces above this moraine ridge reported 11.3 ± 0.8 ka (JO-09) and 13.1 ± 0.9 ka (JO-10), respectively. The innermost sampled boulder (JO-13) gave an age of 0.7 ± 0.2 ka (ca. 1300 CE), while the boulder collected from the lowest polished surface (JO-11) reported a slightly older age of 1.0 ± 0.2 ka (ca. 1100 CE).

4.2.2. The BAE glacier

Considering their altitude and spatial distribution, the CRE results show a logical geochronological pattern indicative of the sequence of glacial oscillations of the BAE Glacier through the Spanish Base Valley.

The youngest CRE ages in the study area were obtained from the glacier forelands unit on the outer ridge of the recent moraine system created by BAE Glacier. Two nearby boulders on the same ridge yielded indistinguishable ages (BAE-03, 0.2 ± 0.3 ka and BAE-02, 0.4 ± 0.2 ka). Another boulder, further away on a more external ridge within the same moraine, gave a slightly older Late Holocene age (BAE-01, 1.9 ± 0.4 ka).

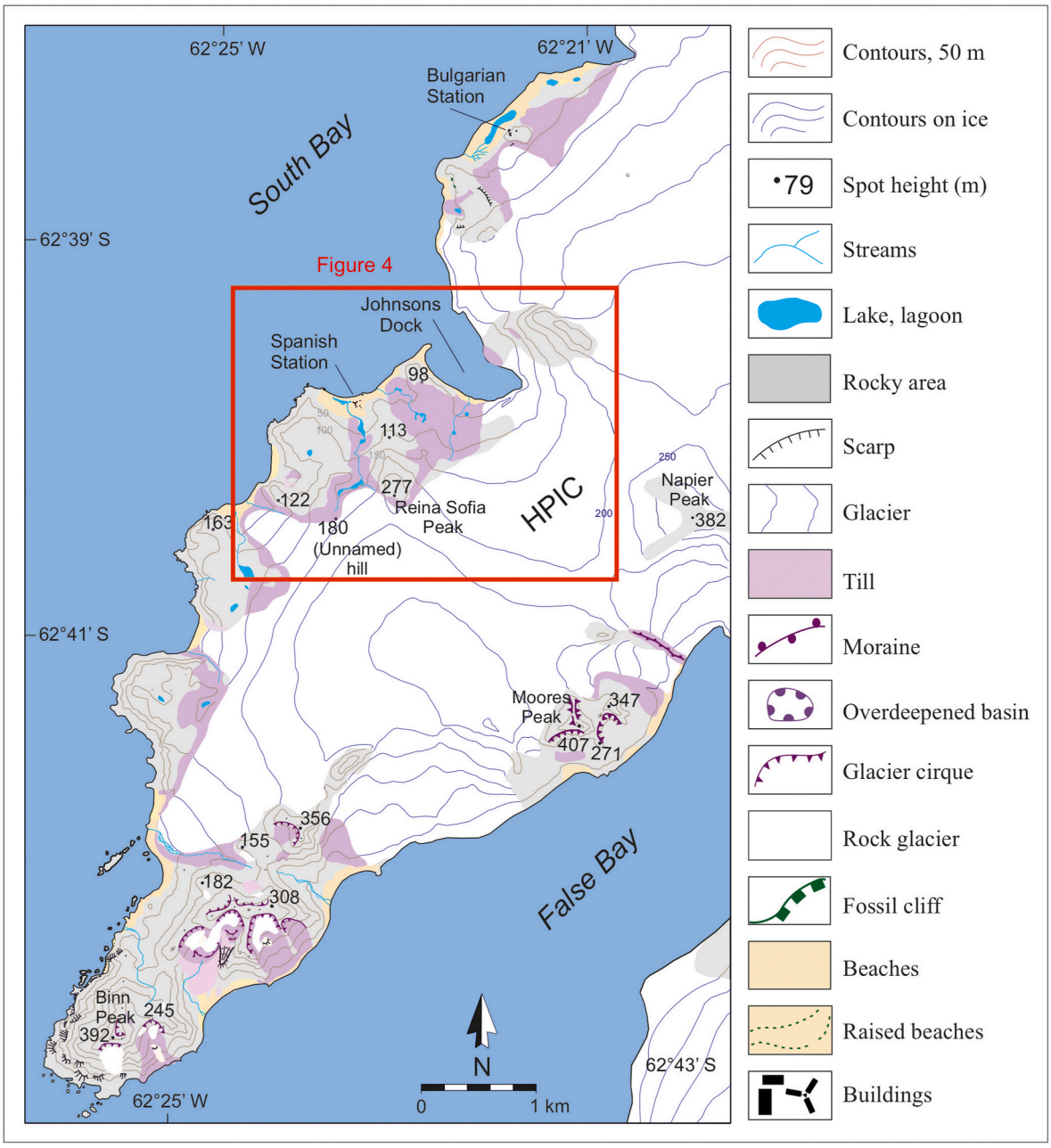

Fig. 3. Geomorphological map of the Hurd Peninsula (shared legend with Fig. 3).

Samples from the high plateaus and ridges yielded Mid-Late Holocene ages at locations closer to the BAE Glacier and much older ones for those further away. Moraine boulders ca. 140–240 m away from the modern glacier snout yielded older ages, as did samples around the unnamed hill, which showed no spatial or elevational patterns (BAE-07, 1.4 ± 0.3 ka; BAE-09, 1.9 ± 0.2 ka; BAE-10, 2.4 ± 0.3 ka; BAE-04, 3.6 ± 0.3 ka; BAE-05, 4.9 ± 0.7 ka; BAE-08; and 6.0 ± 0.5 ka) and those from the inner part of the valley (BAE-14, 4.5 ± 0.5 ka and BAE-13, 4.6 ± 0.4 ka).

The polished and striated glacial surfaces on the western slope of the unnamed hill yielded much older ages than the previous units. The highest sample reported an older age (BAE-12, 14.5 ± 1.1 ka) than the lower sample, which was also closer to the modern margins of the HPIC (BAE-11, 12.1 ± 0.8 ka). The polished bedrock samples on the western slope of Reina Sofia Peak followed a logical vertical sequence, with an LGM age at the upper part of the slope (BAE-21, 20.2 ± 1.4 ka) and a Mid-Holocene age in the middle of the slope (BAE-22, 6.9 ± 0.9 ka).

Finally, the mountain slopes and valley floor samples reflect the deglaciation sequence of the valley sides, with younger ages with decreasing elevation (Fig. 4). The highest glacially abraded surface surrounding the eastern slope of Radio Peak yielded the oldest age (BAE-16, 31.8 ± 2.2 ka), with younger ages at decreasing elevations (BAE-18, 11.3 ± 0.8 ka; BAE-17, 16.0 ± 1.3 ka; BAE-15, 18.4 ± 1.2 ka). The lowest moraine boulders yielded younger, Mid-Holocene ages (BAE-19, 7.5 ± 0.7 ka and BAE-20, 7.8 ± 0.6 ka).

4.3. *Lichenometric dating*

The average length of the longest axis of the ten largest *Rh. geographicum* thalli from site BAE-LICHEN-1 was 31.2 mm, which implies a minimum age of 80–85 years (1938-1933 ± 12 CE) for moraine 1 if the 0.48 mm yr^{-1}growth rate (the average for 1991–2015; Sancho et al., 2017) is considered (Fig. 4). The surface exposure age increases to 104–109 years (1914-1909 ± 12 CE), if we consider the minimum

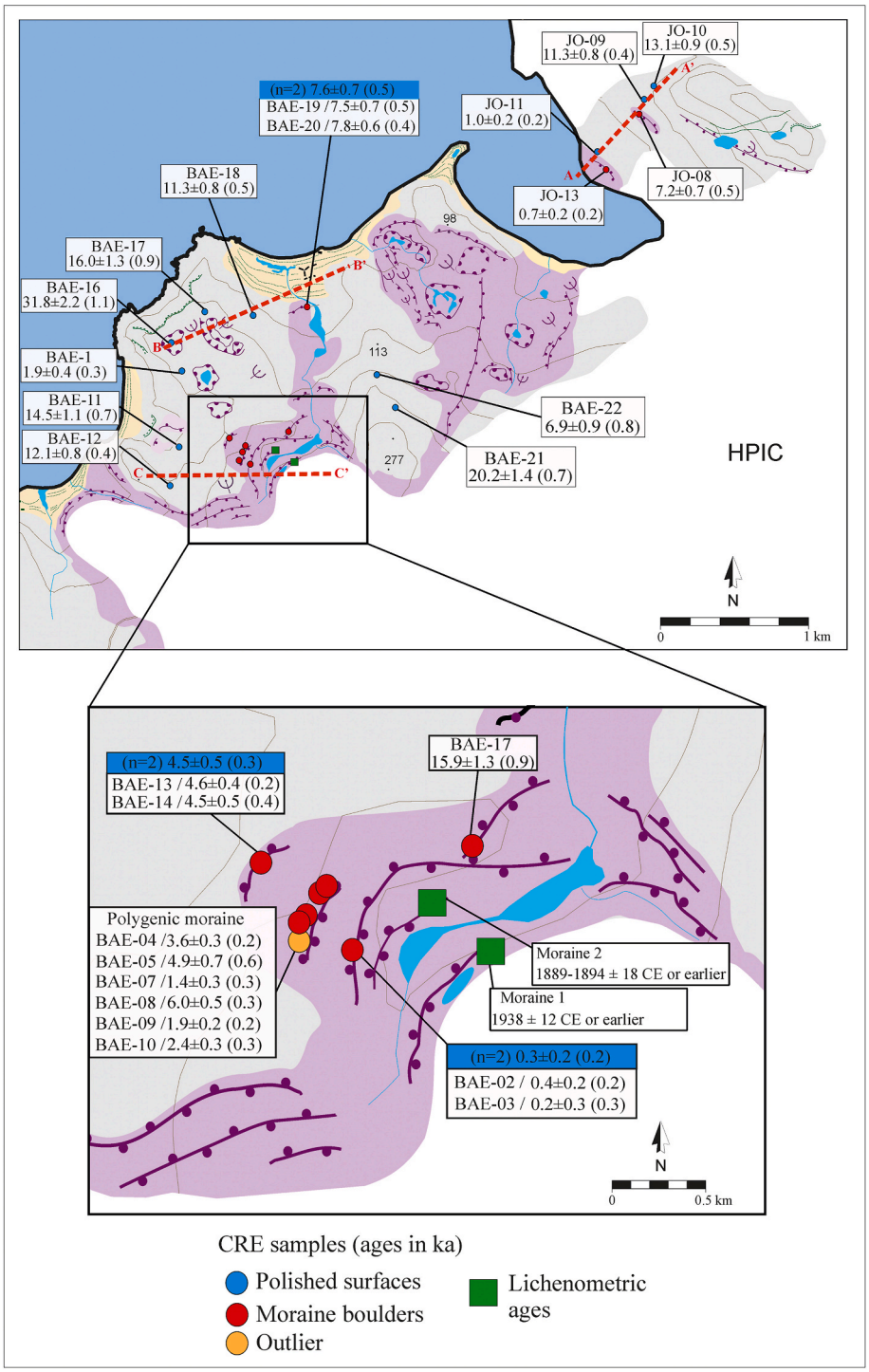

Fig. 4. Main glacial features in the study area, together with the results of CRE dating and lichenometry. The figure includes the location of the transects shown in Fig. 6; the legend is the same as in Fig. 3.

growth rate of 0.35 mm yr^{-1} observed in recent years (2002–2015; Sancho et al., 2017). At BAE-LICHEN-2 on moraine 2, the average length of the longest axis was 52.2 mm, which yields a minimum age of 124–129 (±18) years (1894-1889 ± 24 CE) if we apply the 0.48 mm yr^{-1} growth rate. In any case, this age would be slightly older if we take into account the lower temperatures and persistent snow cover of recent years, which implies lower growth rates.

5. Discussion

The extensive glaciation of Antarctica, with 99.6% of its surface being ice-covered (Convey, 2010), severely restricts the availability of terrestrial paleoenvironmental evidence of deglaciation history in the continent's limited ice-free areas. In this study, we combined direct surface exposure dating of polished surfaces and moraine boulders with lichenometry performed on the most recent moraine ridges to reconstruct the spatial and temporal patterns of glacial thinning and horizontal retreat on the Hurd Peninsula in Livingston Island.

5.1. Glacial oscillations in the Hurd Peninsula

Applying CRE dating in areas surrounding polar ice sheets is challenging due to the limited preservation of previously exposed bedrock and landforms beneath cold (or polythermal)-based glacier systems (Small et al., 2019). In this study, most samples followed the expected chronostratigraphic sequence and had logical geomorphological implications. We infer three main stages in the deglaciation of the area based on the distribution of CRE ages and the lichenometric data across the Hurd Peninsula (Fig. 6).

5.1.1. Deglaciation of the highest surfaces (ca. 32-18 ka)

Our dates yielded a deglaciation age of 31.8 ± 2.2 ka (BAE-16), predating the global LGM, while others suggested ice thinning during the LGM, including the ages of the bedrock surface on the other side of the slope (BAE-21; 20.2 ± 1.4 ka), and the upper land surface of Spanish Base Valley (BAE-15; 18.4 ± 1.2 ka). We cannot completely rule out the possibility that sample BAE-16 may retain some nuclide inheritance with an apparent age older than the actual age of deglaciation at this site. Ages from samples BAE-21 and BAE-15 are consistent with the deglaciation of the summit surface (at ca. 250 m asl) of Reina Sofia Peak, adjacent to the margin of the HPIC, which was deglaciated at 17–18.5 ka (Fernández-Fernández et al., 2021).

5.1.2. Deglaciation of the valleys (ca. 18-7 ka)

Exposure ages at elevations of ca. 80–95 m asl (BAE-11, BAE-17) suggested that the ice volume in the western part of Livingston Island followed the long-term deglaciation trend since the LGM, and by 16-14.5 ka the lower plateau of the Hurd Peninsula was already ice-free. This glacial shrinking pattern continued until the Early Holocene. The mid-low slopes of Spanish Base Valley became ice-free at 12-11 ka (BAE-12, BAE-18), while the glacier left the valley floor after forming a moraine ca. 7.5–7.8 ka (BAE-19, BAE-20). While the ice tongue descending through Spanish Base Valley disappeared at that time, lobes of the ice cap likely persisted in the upper areas encircling Reina Sofia Peak, as revealed by polished surfaces at the base of its western slope that became ice-free at 6.9 ± 0.9 ka (BAE-22).

Ice thinning also occurred in Johnsons Glacier Valley at 13-11 ka (JO-09, JO-10). On the valley floor, a moraine boulder at the foot of the slope dated to 7.2 ± 0.7 ka (JO-08) may indicate that glacier shrinkage continued throughout the Early-Mid Holocene, with the final retreat of the glacier at this time, but it may also indicate the definitive stabilisation of the moraine, which is located under a very active slope.

5.1.3. Neoglacial oscillations (from ca. 7 ka to present-day)

There were no large-scale glacial advances in the area during the second half of the Holocene. Evidence shows that the BAE Glacier was relatively larger during the Neoglacial period when the lobe deposited a moraine at ca. 4.5 ka (BAE-13, BAE-14). Assuming this average age to be valid implies that the sample BAE-08 (6.0 ± 0.5 ka) is thus considered an outlier. In any case, this period was followed by a period of relative glacier stabilisation, favouring the formation of a polygenic moraine, as suggested by the six CRE samples aged between 4.9 ± 0.7 ka (BAE-05) and 1.4 ± 0.3 ka (BAE-07).

The BAE Glacier has formed an extensive moraine system over the last several centuries, with two distinct moraine ridges dated by CRE and lichenometry. CRE ages of the external moraine ridge (0.3 ± 0.2 ka; BAE-02, BAE-03) indicated that the maximum advance of the glacier was during the Little Ice Age (LIA). Another sample taken from this ridge in a more external position gave a significantly older age of 1.9 ± 0.4 ka (BAE-01), suggesting that some sectors of the moraine may be polycyclic.

Lichenometry was applied to the internal moraine system and showed that the two minor arcs were abandoned by the glacier between the late 19th and mid-20th century (from the outermost to innermost). Applying the lower growth rate observed in years of longer snow cover duration (i.e., 0.35 mm yr^{-1}) implies a minimum surface exposure age of 164–169 (±24) years (1854-1849 ± 18 CE; Table 2), which is potentially consistent with the last pulse of the LIA in other areas. Interestingly, this moraine rests on a set of moraines that were ^{10}Be dated to the 17th century (Figs. 5 and 6), which has been traditionally considered the maximum advance of the LIA in the SSI (Palacios et al., 2020; Herediа-Barión et al., 2023a). CRE ages also confirm that the Johnsons Glacier has undergone recent oscillations. Exposure ages obtained close to the present glacier terminus (JO-11, JO-13) suggest that it has not experienced major advances during the last millennium, but minor advances and retreats must have occurred during the last several centuries as evidenced by the presence of minor moraine ridges within about 200 m of the glacier margin.

5.2. Deglacial history within the regional context

Nunataks on the Hurd Peninsula have recently provided some of the oldest CRE ages in the northern sector of the Antarctic Peninsula (Fernández-Fernández et al., 2021; Oliva et al., 2019a,b), demonstrating that the entire SSI archipelago was heavily glaciated during the last glacial cycle (John and Sugden, 1972; Nývlt et al., 2020). During the maximum ice extent of the last glacial cycle, a marine-based ice cap centred between Robert and Greenwich islands extended multiple kilometres offshore, connecting with the ice cap extending over the Antarctic Peninsula and the rest of the continent across the southern fringe of the archipelago (Ó Cofaigh et al., 2014). Previous studies have provided evidence that this ice cap began to shrink during the LGM, as indicated by CRE ages from nunataks on Livingston Island, from both the Hurd Peninsula at ca. 22–25 ka (^{10}Be) (Fernández-Fernández et al., 2021) and from the Byers Peninsula at ca. 26-19 ka (^{36}Cl) (Oliva et al., 2019a,b). However, sample BAE-16 from the present study yielded a deglaciation age of 31.8 ± 2.2 ka - the oldest in the dataset - tentatively suggesting that the onset of ice shrinkage in the northern Antarctic Peninsula might have begun before the LGM, exposing the highest coastal areas further away from ice accumulation areas. The sample was collected at the highest divide between the Spanish Base and Argentine valleys, distant from the ice cap, and it would have been the first land surface to be exposed when the ice began to thin. However, a single old age must be interpreted with caution as samples with nuclide inheritance have been reported in this peninsula in areas with very low ice-flow dynamics of the cold-based glaciers on gentle slopes (Fernández-Fernández et al., 2021). Further multi-proxy data should shed more light on this issue. In any case, there is widespread evidence from terrestrial records that deglaciation was underway across the Antarctic Peninsula during the global LGM at ca. 22–27 ka (^{10}Be), as reported on Alexander Island (Bentley et al., 2006; Johnson et al., 2012), as well as from marine proxy data that also confirm retreating ice masses at ca. 22–24 ka cal BP (Collins et al., 2012; Hillenbrand et al., 2010; Smith et al., 2011). On the Hurd Peninsula, samples from the summit plateaus (BAE-15, BAE-21) also confirmed the pattern of ice shrinkage during the late LGM between ca. 20 and 18 ka (Fig. 7).

CRE dates of nunataks on the Hurd Peninsula indicated that the HPIC continued the thinning trend between ca. 18 and 13 ka (^{10}Be) (Fernández-Fernández et al., 2021), which favoured the shrinkage of the ice cap and the retreat of ice masses and streams. Ages from the lower plateau at elevations of ca. 80–95 m asl (14.5 ± 1.1 and 15.9 ± 1.3 ka; BAE-11 and BAE-17) confirmed the progressive reduction of the ice volume stored on the western part of Livingston Island. Marine records also provide evidence of the shrinking ice masses at this time; glaciomarine sediments revealed that some of the largest bays in the SSI began to be deglaciated at 17 ka cal BP (Yoon et al., 1997) and by 14.8–14.1 ka cal BP glaciers were no longer grounded (Milliken et al., 2009; Simms et al., 2011). The trend towards glacial shrinking accelerated between ca. 14 and 13 ka, as observed in many areas across the Antarctic Peninsula (Bentley et al., 2014; Small et al., 2019), which reinforces the hypothesis that this portion of the continent may have been a major

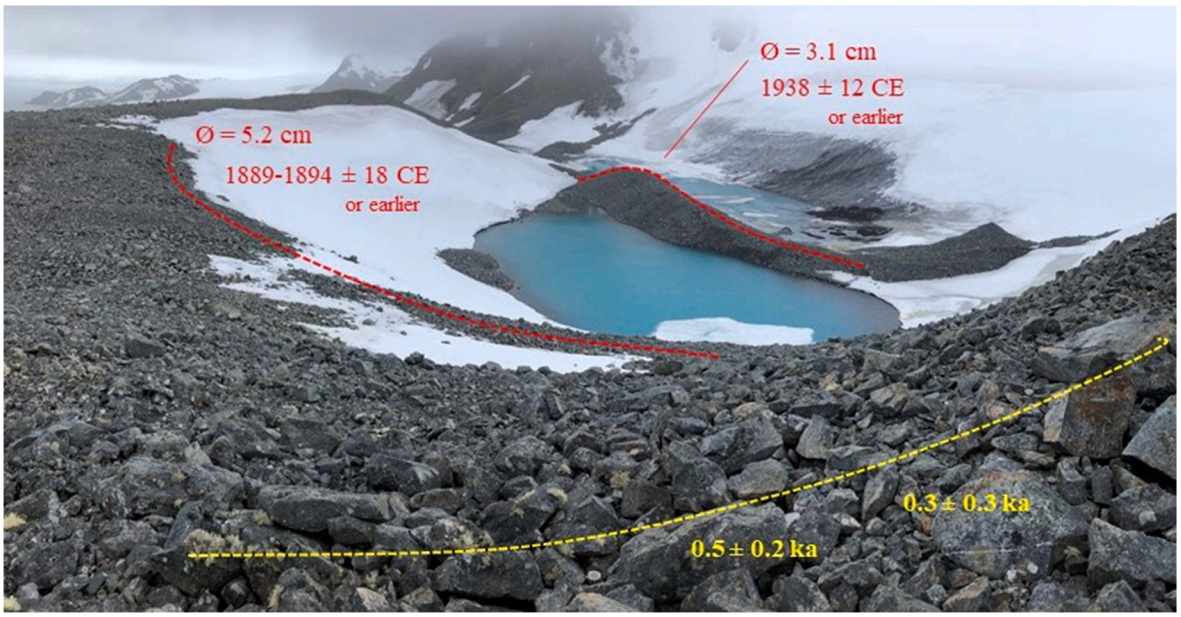

Fig. 5. Chronology of the recent moraine system built by the BAE Glacier based on the minimum ages provided by lichenometric data (red) and CRE results (yellow). The dashed lines represent the moraine crests.

source of the MWP-1a massive meltwater release event (Fernández-Fernández et al., 2021).

Glacial evidence from both the Johnsons and Spanish Base valleys suggests that glacial shrinking continued from the Late Glacial to the beginning of the Holocene on the Hurd Peninsula. Four CRE ages from ice-moulded surfaces indicated ice thinning at the transition between the Late Glacial and the Holocene at 13-11 ka (JO-09, JO-10, BAE-12 and BAE-18). This trend favoured the retreat of ice masses, as suggested by marine records, which indicated that open marine conditions prevailed in the Bransfield Strait and Maxwell Bay by 10.1 ka cal BP (Simms et al., 2011). At the onset of the Holocene, the islands of the SSI archipelago were largely covered by independent ice caps (Ingólfsson et al., 1998), and ice-free areas were restricted to the highest summit surfaces and lowlands located further away from the glacier accumulation centres (Fernández-Fernández et al., 2021). During the Early Holocene, warmer climate conditions in the northern Antarctic Peninsula favoured the retreat of ice masses (Bentley et al., 2009), and during this period both marine and terrestrial records indicate the onset of ice-free conditions in low-lying areas distant from ice cap accumulation zones. Sedimentation rates and biological proxies point to a period of rapid glacial retreat between 10.1 and 8.2 ka cal BP in Maxwell Bay (Milliken et al., 2009), which also favoured the formation of raised beaches (Fretwell et al., 2010) and the appearance of lakes in the present-day ice-free areas (Oliva et al., 2019b; Oliva et al., 2016b; Roberts et al., 2017; Tatur et al., 1996; Toro et al., 2013; Watcham et al., 2011).

This long-term trend continued throughout the Early and the Mid-Holocene but likely stopped around ca. 7.2–7.8 ka (JO-08, BAE-19 and BAE-20), when the stabilisation of moraine boulders in both valleys may indicate a period of glacial standstill. Some SSI ice caps had minor advances at this time, including on Potter Peninsula between 8.2 and 7.0 ka (Heredia-Barión et al., 2023b) and Fildes Peninsula between ca. 7.4 and 6.6 ka cal BP (Heredia-Barión et al., 2023a). On the Hurd Peninsula, glacially polished surfaces dated to 6.9 ± 0.9 ka (BAE-22) suggest that the pause in glacial thinning was transient and that ice masses resumed their retreat shortly thereafter. This pattern is widely documented across the SSI, such as in the Fildes Peninsula, where CRE ages indicated that the northern plateau was deglaciated at ca. 7.0-6.0 ka (Oliva et al., 2023) and by 5.3 ka cal BP the configuration of the Collins Ice Cap was similar to the present (Heredia Barión et al., 2023a). The intense deglaciation at ca. 7.0 ka cal BP resulted in the highest glacio-isostatic rebound rates in the archipelago (Fretwell et al., 2010; Hall, 2010), which expanded the incipient ice-free environments as was observed on the Byers Peninsula (Oliva et al., 2016a; Ruiz-Fernández and Oliva, 2016). While the uplift of raised beaches during the Late Holocene in other areas of the SSI, such as the Fildes Peninsula, has been tentatively linked to the timing of moraine development (Hall, 2003; John and Sugden, 1972; Simms et al., 2021), this relationship has not been successfully explored on Livingston Island. Some studies, however, have dated local glacial advances over the last few millennia from the distribution of moraines and erratic boulders on raised beaches, such as on the Byers Peninsula (Palacios et al., 2020).

The upper valley of the BAE Glacier preserves geomorphic evidence that suggest potential neoglacial oscillations. The different number of CRE samples available (2 from Johnsons Glacier vs. 11 samples from the BAE Glacier) may explain the differing neoglacial chronologies in the two valleys, together with the local configuration of the relief. Johnsons Glacier is constrained by near-vertical walls characteristic of glacial valleys and its proglacial zone, which is submerged in the sea, hinders the preservation of neoglacial landforms. In contrast, the foreland of the BAE Glacier is ideal for the preservation of moraines because they were deposited on stable, flat, rocky steps. As a result, this area contains some of the most complete neoglacial sequences in the Antarctic Peninsula region.

Increasing climate variability has resulted in several small glacier advances and retreats since the Mid-Holocene. The lobe of the BAE Glacier expanded along the valleys, forming moraines where the advancing ice was blocked by relief, such as at the unnamed hill, which favoured the accumulation of moraine boulders that were superimposed with each glacier advance. This explains the range of ages of the moraine ridges distributed upvalley from this hill, from 4.9 to 1.4 ka, with the youngest being closest to the present glacier front. Neoglacial ages similar to those obtained in the forelands of the BAE Glacier area have been found on the Byers Peninsula, on the western fringe of Livingston Island. The central plateau of the Byers Peninsula, which is the largest ice-free environment in the SSI, was deglaciated at 7–8 ka (Oliva et al., 2016a), and neoglacial moraines developed at 4.1 ± 0.5 and 1.0 ± 0.2 ka (Palacios et al., 2020). Similarly, other large ice-free areas in the SSI show evidence of glacier expansion with moraine formation during the Late Holocene, such as the Fildes Peninsula, where multi-proxy data records indicate glacial advances between ca. 5.3 and 2.2, at 1.7-1.5,

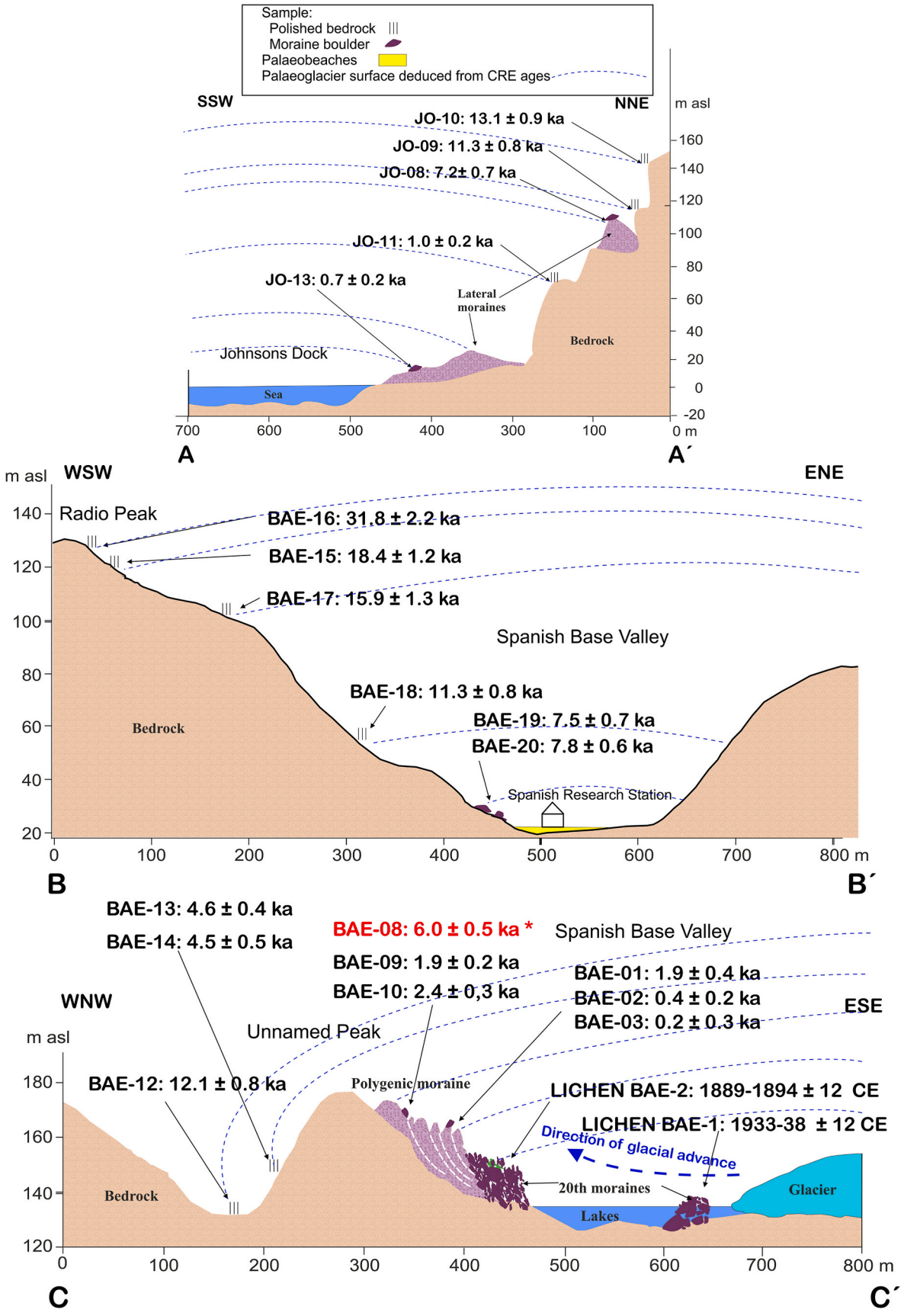

Fig. 6. CRE ^{10}Be ages (outliers are represented in red) along different deglaciation transects shown in Fig. 4.

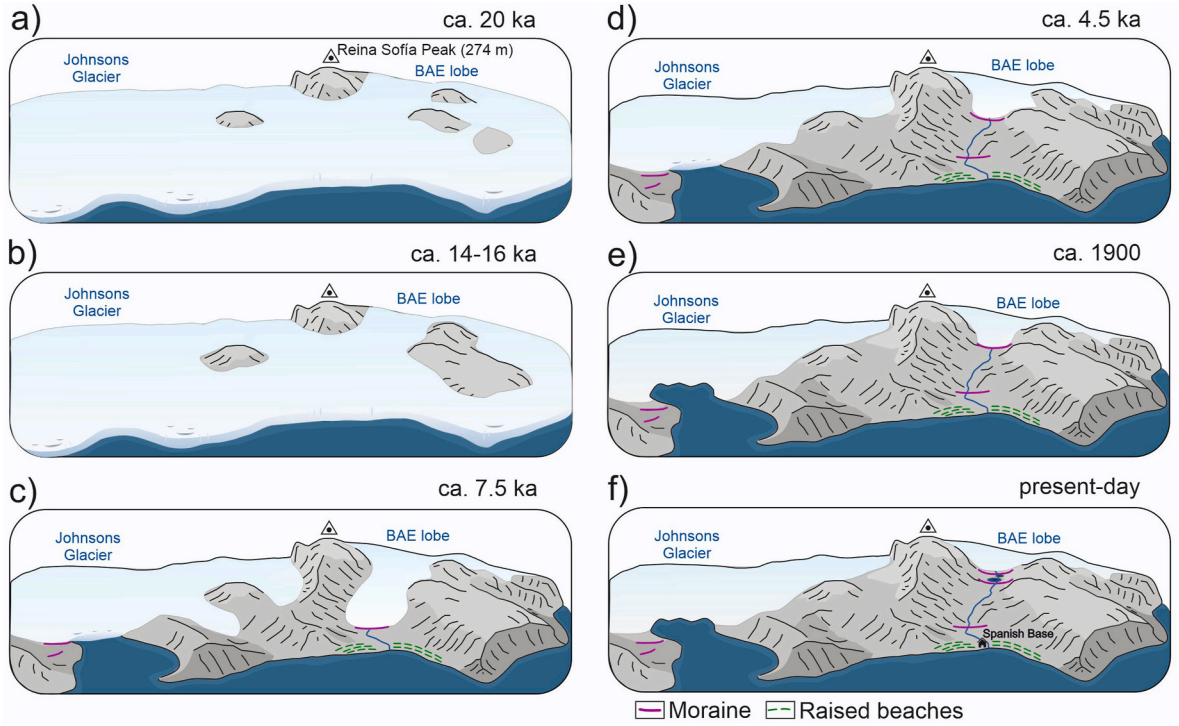

Fig. 7. Main geochronological stages according to CRE and lichenometric dating.

possibly at ca. 1.3-0.7 and after <0.7 cal ka BP (Heredia-Barión et al., 2023a), and CRE ages from its northern plateau suggest two neoglacial advances with the formation of polygenic moraines at ca. 4.6 and 1 ka (Oliva et al., 2023). Elsewhere on King George Island, on the Potter Peninsula, neoglacial advances occurred at 1.7–1.4 cal ka BP and during the LIA at 0.5–0.1 cal ka BP (Heredia-Barión et al., 2023b). Similar Late Holocene glacial advances have been found in many other sectors of the Antarctic Peninsula (e.g. Čejka et al., 2020; Kaplan et al., 2020).

The timing and magnitude of the LIA in the Antarctic Peninsula have been extensively discussed (Palacios et al., 2020; Heredia-Barión et al., 2023a) and remain a matter of debate. We documented several advances of the BAE Glacier during the LIA (14th-19th centuries) using CRE dating. These advances were always more limited than previous neoglacial advances and reached their maximum extent during the 17th century, although the glacier experienced several other advances and retreats of lesser magnitude. On the Fildes Peninsula, the largest glacier advance during the LIA occurred around the 14th century (Hall, 2007; Heredia-Barión et al., 2023a). In other areas of the Antarctic Peninsula, the maximum extent of the LIA took place between the 14th and 17th centuries, as revealed by glacial sediments deposited on well-dated moraines and by direct CRE dating of moraines, such as on Greenwich Island, Joinville Island, James Ross Island and Marguerite Bay (Guglielmin et al., 2016; Kaplan et al., 2020; Simms et al., 2021).

The timing of the last two advances of the BAE Glacier was established through lichenometry. The site BAE-LICHEN-2 indicates that the last advance of note occurred in the late 19th century (probably at 1889–1894 ± 18 CE or earlier). The lichenometry site BAE-LICHEN-1, located on the younger moraine, indicates a glacial advance of more limited scope during the first decades of the last century (probably at 1938 ± 12 CE or earlier). However, it is likely that the glacier snout remained in the vicinity of this moraine for several decades.

6. Conclusions

We reconstructed the spatial and temporal patterns of glacier thinning and retreating in the small ice-free area of the Hurd Peninsula by integrating absolute surface exposure dating and lichenometry. The oldest age tentatively points to thinning of the ice cap likely before the LGM at ca. 31.8 ka, exposing the highest coastal surfaces of the peninsula, which however needs to be verified by additional investigations. Twenty-two further, chronologically consistent results indicated that the deglaciation process accelerated at ca. 20-18 ka, resulting in the complete disappearance of ice from the high plateaus between 16 and 14 ka. The HPIC then may have remained relatively stable, with minor oscillations of the ice masses, until the Mid-Holocene, when neoglacial advances occurred at ca. 4.5 ka and between this time and the LIA forming a polygenic moraine. The last of these advances, and subsequent stabilisation, occurred during the late 19th and early 20th century, according to lichenometric data.

These results provide important insights into the major periods of glacial change on the Antarctic Peninsula and agree well with the few other glacial chronologies in the region. The study also highlights the importance of combining different absolute dating approaches and integrating them with data from other natural archives to better link glacier responses to climate variability at different time scales in polar regions.

7. Author contributions

All authors have participated in (i) conception and design, or analysis and interpretation of the data; (ii) drafting the article or revising it critically for important intellectual content; and (iii) approval of the final version. This manuscript has not been submitted to, nor is under review at, another journal or other publishing venue.

8. Participation of authors in the work

All the authors have been actively involved in the investigation presented in this work.

1 Marc Oliva, coordination of all phases of the research and writing of a first draft of the manuscript, leading the fieldwork, geomorphological analysis, sampling and data processing.<a name = "Line_supportingmanuscript_5">

2. David Palacios. Fieldwork, geomorphological analysis, discussion of the results, contribution to the geomorphological mapping and writing.
3. Leopoldo G. Sancho. Fieldwork, lichenometric analysis, discussion of the results.
4. José M. Fernández-Fernández. Laboratory tasks (sample processing, exposure age calculations), discussion of the results and contribution to the writing.
5. Attila Çiner. Discussion of the results and contribution to the writing.
6. Marcelo Fernandes. Laboratory tasks (sample processing), discussion of the results and contribution to the writing.
7. Julia García-Oteyza. Laboratory tasks (sample processing), and contribution to the writing.
8. M. Akif Sarıkaya. Laboratory tasks (sample processing), discussion of the results and contribution to the writing.
9. Enrique Serrano. Fieldwork, geomorphological analysis, discussion of the results, geomorphological mapping and writing.
10. Amaneh Kaveh-Firouz. Laboratory tasks (sample processing), discussion of the results and contribution to the writing.
11. Augusto Pérez-Alberti. Fieldwork, geomorphological analysis and contribution to the writing.
12. Irene Schimmelpfennig. Supervision of the whole process of the sample processing and interpretation of the results. Thorough correction of the manuscript.
13 Gonçalo Vieira. Discussion of the results and contribution to the writing.
14. Josep Bonsoms. Geochronological analysis, contribution to the geomorphological mapping and writing.
15. Dermot Antoniades. Interpretation of the results and contribution to the revision of the manuscript.
16 ASTER Team. AMS measurements of the ^{36}Cl samples.

Declaration of competing interest

The authors declare that they have no known competing financial interests or personal relationships that could have appeared to influence the work reported in this paper.

Acknowledgements

This research was framed within the NUNANTAR project (PTDC/CTA-GFI/32002/2017–32002) funded by the Portuguese Science Foundation, and complements the topics studied in the NEOGREEN (PID2020-113798GB-C31) and NEOICE (PID2020-113798GB-C32) projects funded by the Spanish Ministry of Economy and Competitiveness. The ^{10}Be measurements were performed at the ASTER AMS National Facility (CEREGE, Aix-en-Provence), supported by the INSU/CNRS and the ANR through the "Projets thématiques d'excellence" programme for the "Équipements d'excellence" ASTER-CEREGE action and the IRD. We also thank the ANTALP (Antarctic, Arctic, Alpine Environments; 2021-SGR-00269) research group and the Portuguese Polar Program (PROPOLAR/FCT) and Spanish Polar Committees for logistical support, and Jesús Ruiz for field assistance.

Data availability

Data will be made available on request.

References

Arche, A., López-Martínez, J., Serrano, E., Martínez de Pisón, E., 1996. Marine landforms and deposits. In: López-Martínez, J., Thomson, M.R.A., Thomson, J.W. (Eds.), Geomorphological Map of Byers Peninsula, Livingston Island, BAS Geomap Series, pp. 34–35, 5–A.

Armstrong, R.A., 2013. Development of areolae and growth of the peripheral prothallus in the crustose lichen Rhizocarpon geographicum: an image analysis study. Symbiosis 60, 7–15.

Arnold, M., Merchel, S., Bourlès, D.L., Braucher, R., Benedetti, L., Finkel, R.C., Aumaître, G., Gottdang, A., Klein, M., 2010. The French accelerator mass spectrometry facility ASTER. Improved performance and developments 268, 1954–1959. https://doi.org/10.1016/j.nimb.2010.02.107.

Balco, G., Stone, J.O., Lifton, N.A., Dunai, T.J., 2008. A complete and easily accessible means of calculating surface exposure ages or erosion rates from ^{10}Be and ^{26}Al measurements. Quat. Geochronol. 3, 174–195. https://doi.org/10.1016/j.quageo.2007.12.001.

Bañón, M., Justel, A., Velázquez, D., Quesada, A., 2013. Regional weather survey on Byers peninsula, Livingston island, South Shetland islands, Antarctica. Antarct. Sci. 25, 146–156. https://doi.org/10.1017/S0954102012001046.

Bentley, M.J., Fogwill, C.J., Kubik, P.W., Sugden, D.E., 2006. Geomorphological evidence and cosmogenic ^{10}Be/^{26}Al exposure ages for the last glacial maximum and deglaciation of the antarctic peninsula ice sheet. Bull. Geol. Soc. Am. 118, 1149–1159. https://doi.org/10.1130/B25735.1.

Bentley, M.J., Hodgson, D.A., Smith, J.A., Cofaigh, C.Ó., Domack, E.W., Larter, R.D., Roberts, S.J., Brachfeld, S., Leventer, A., Hjort, C., Hillenbrand, C.D., Evans, J., 2009. Mechanisms of Holocene palaeoenvironmental change in the antarctic peninsula region. Holocene 19, 51–69. https://doi.org/10.1177/0959683608096603.

Bentley, M.J., Ocofaigh, C., Anderson, J.B., Conway, H., Davies, B., Graham, A.G.C., Hillenbrand, C.D., Hodgson, D.A., Jamieson, S.S.R., Larter, R.D., Mackintosh, A., Smith, J.A., Verleyen, E., Ackert, R.P., Bart, P.J., Berg, S., Brunstein, D., Canals, M., Colhoun, E.A., Crosta, X., Dickens, W.A., Domack, E., Dowdeswell, J.A., Dunbar, R., Ehrmann, W., Evans, J., Favier, V., Fink, D., Fogwill, C.J., Glasser, N.F., Gohl, K., Golledge, N.R., Goodwin, I., Gore, D.B., Greenwood, S.L., Hall, B.L., Hall, K., Hedding, D.W., Hein, A.S., Hocking, E.P., Jakobsson, M., Johnson, J.S., Jomelli, V., Jones, R.S., Klages, J.P., Kristoffersen, Y., Kuhn, G., Leventer, A., Licht, K., Lilly, K., Lindow, J., Livingstone, S.J., Masse, G., McGlone, M.S., McKay, R.M., Melles, M., Miura, H., Mulvaney, R., Nel, W., Nitsche, F.O., O'Brien, P.E., Post, A.L., Roberts, S.J., Saunders, K.M., Selkirk, P.M., Simms, A.R., Spiegel, C., Stolldorf, T.D., Sugden, D.E., van der Putten, N., van Ommen, T., Verfaillie, D., Vyverman, W., Wagner, B., White, D.A., Witus, A.E., Zwartz, D., 2014. A community-based geological reconstruction of Antarctic ice sheet deglaciation since the last glacial maximum. Quat. Sci. Rev. 100, 1–9. https://doi.org/10.1016/j.quascirev.2014.06.025.

Borchers, B., Marrero, S., Balco, G., Caffee, M., Goehring, B., Lifton, N., Nishiizumi, K., Phillips, F., Schaefer, J., Stone, J., 2016. Geological calibration of spallation production rates in the CRONUS-Earth project. Quat. Geochronol. 31, 188–198. https://doi.org/10.1016/j.quageo.2015.01.009.

Braucher, R., Guillou, V., Bourlès, D.L., Arnold, M., Aumaître, G., Keddadouche, K., Nottoli, E., 2015. Preparation of ASTER in-house ^{10}Be/^{9}Be standard solutions. Nucl. Instrum. Methods Phys. Res. B 361, 335–340. https://doi.org/10.1016/j.nimb.2015.06.012.

Briner, J.P., Cuzzone, J.K., Badgeley, J.A., Young, N.E., Steig, E.J., Morlighem, M., Schlegel, N.J., Hakim, G.J., Schaefer, J.M., Johnson, J.V., Lesnek, A.J., Thomas, E.K., Allan, E., Bennike, O., Cluett, A.A., Csatho, B., de Vernal, A., Downs, J., Larour, E., Nowicki, S., 2020. Rate of mass loss from the Greenland Ice Sheet will exceed Holocene values this century. Nature 586, 70–74. https://doi.org/10.1038/s41586-020-2742-6.

Čejka, T., Nývlt, D., Kopalová, K., Bulínová, M., Kavan, J., Lirio, J.M., Coria, S.H., van de Vijver, B., 2020. Timing of the neoglacial onset on the north-eastern antarctic peninsula based on lacustrine archive from lake anónima, vega island. Glob. Planet. Change 184, 103050. https://doi.org/10.1016/j.gloplacha.2019.103050.

Chmeleff, J., von Blanckenburg, F., Kossert, K., Jakob, D., 2010. Determination of the ^{10}Be half-life by multicollector ICP-MS and liquid scintillation counting. Nucl. Instrum. Methods Phys. Res. B 268, 192–199. https://doi.org/10.1016/j.nimb.2009.09.012.

Clark, P., Dyke, A., Shakun, J., Carlson, A., Clark, J., Wohlfarth, B., Mitrovica, J., Hostetler, S., McCabe, A., 2009. The last glacial maximum. Science 325, 710–714. https://doi.org/10.1126/science.1172873.

Collins, L.G., Pike, J., Allen, C.S., Hodgson, D.A., 2012. High-resolution reconstruction of southwest Atlantic sea-ice and its role in the carbon cycle during marine isotope stages 3 and 2. Paleoceanography 27, 1–17. https://doi.org/10.1029/2011PA002264.

Convey, P., 2010. Terrestrial biodiversity in Antarctica - recent advances and future challenges. Polar Sci 4, 135–147. https://doi.org/10.1016/j.polar.2010.03.003.

Correia, A., Oliva, M., Ruiz-Fernández, J., 2017. Evaluation of frozen ground conditions along a coastal topographic gradient at Byers Peninsula (Livingston Island, Antarctica) by geophysical and geoecological methods. Catena 149, 529–537. https://doi.org/10.1016/j.catena.2016.08.006.

Denton, G.H., Anderson, R.F., Toggweiler, J.R., Edwards, R.L., Schaefer, J.M., Putnam, A.E., 2010. The last glacial termination. Science 328, 1652–1656. https://doi.org/10.1126/science.1184119.

Fernández-Fernández, J.M., Palacios, D., Andrés, N., Schimmelpfennig, I., Brynjólfsson, S., Sancho, L.G., Zamorano, J.J., Heiðmarsson, S., Sæmundsson, Þ., ASTER Team, 2019. A multi-proxy approach to Late Holocene fluctuations of Tungnahryggsjökull glaciers in the Tröllaskagi peninsula (northern Iceland). Sci. Total Environ. 664, 499–517. https://doi.org/10.1016/j.scitotenv.2016.12.030.

Fernández-Fernández, J.M., Oliva, M., Palacios, D., García-Oteyza, J., Navarro, F.J., Schimmelpfennig, I., Léanni, L., ASTER Team, 2021. Ice thinning on nunataks during the last glacial termination in the antarctic peninsula according to cosmic-ray exposure dating: evidence and uncertainties. Quat. Sci. Rev. 264, 107029. https://doi.org/10.1016/j.quascirev.2021.107029.

Ferreira, A., Vieira, G., Ramos, M., Nieuwendam, A., 2017. Ground temperature and permafrost distribution in Hurd Peninsula (Livingston Island, Maritime Antarctic): an assessment using freezing indexes and TTOP modelling. Catena 149, 560–571. https://doi.org/10.1016/j.catena.2016.08.027.

Fretwell, P.T., Hodgson, D.A., Watcham, E.P., Bentley, M.J., Roberts, S.J., 2010. Holocene isostatic uplift of the South Shetland islands, antarctic peninsula, modelled from raised beaches. Quat. Sci. Rev. 29, 1880–1893. https://doi.org/10.1016/j.quascirev.2010.04.006.

Giralt, S., Hernández, A., Pla-Rabés, S., Antoniades, D., Toro, M., Granados, I., Oliva, Marc, 2020. Holocene environmental changes deduced from lake sediments. In: Oliva, M., Ruiz-Fernández, J. (Eds.), Past Antarctica. Elsevier, pp. 51–68.

Golledge, N., Everest, J.D., Bradwell, T., Johnson, J.S., 2010. Antarctic Peninsula: size-frequency studies, growth rates and snowpatches. Geogr. Ann. A (9), 111–123.

González-Herrero, S., Barriopedro, D., Trigo, R.M., López-Bustins, J.A., Oliva, M., 2022. Climate warming amplified the 2020 record-breaking heatwave in the Antarctic Peninsula. Commun. Earth Environ. 3, 122. https://doi.org/10.1038/s43247-022-00450-5.

Guglielmin, M., Convey, P., Malfasi, F., Cannone, N., 2016. Glacial fluctuations since the 'medieval warm period'' at rothera point (western antarctic peninsula). Holocene 26, 154–158. https://doi.org/10.1177/0959683615596827.

Hall, B.L., 2003. An overview of late pleistocene glaciation in the South Shetland islands. En Antarctic Peninsula Climate Variability: Historical and Paleoenvironmental Perspectives 79, 103–113.

Hall, B.L., 2007. Late-holocene advance of the Collins ice cap, king George island, South Shetland islands. Holocene 17, 1253–1258.

Hall, B.L., 2009. Holocene glacial history of Antarctica and the sub-Antarctic islands. Quat. Sci. Rev. 28, 2213–2230. https://doi.org/10.1016/j.quascirev.2009.06.011.

Hall, B.L., 2010. Holocene relative sea-level changes and ice fluctuations in the South Shetland Islands. Glob. Planet Change 74, 15–26. https://doi.org/10.1016/j.gloplacha.2010.07.007.

Heredia-Barión, P., 2019. Paleoenvironmental Evolution of On-Shore Ice-free Areas Around Maxwell Bay, King George Island, South Shetland Islands. Universität Bremen. PhD Thesis.

Heredia-Barión, P., Roberts, S.J., Spiegel, C., Binnie, S.A., Wacker, L., Davies, J., Gabriel, I., Jones, V.J., Blockley, S., Pearson, E.J., Foster, L., Davies, S.J., Roland, T. P., Hocking, E.P., Bentley, M.J., Hodgson, D.A., Hayward, C.L., McCulloch, R.D., Strelin, J.A., Kuhn, G., 2023a. Holocene deglaciation and glacier readvances on the Fildes Peninsula and King George Island (Isla 25 de Mayo), South Shetland Islands, NW Antarctic Peninsula. Holocene 33, 636–658. https://doi.org/10.1177/09596836231157059.

Heredia-Barión, P., Strelin, J.A., Roberts, S.J., Spiegel, C., Wacker, L., Niedermann, S., Bentley, M.J., Pearson, E.J., Czalbowski, N.T.M., Davies, S.J., Schnetger, B., Grosjean, M., Arcusa, S., Perren, B., Hocking, E.P., Kuhn, G., 2023b. The impact of Holocene deglaciation and glacial dynamics on the landscapes and geomorphology of potter peninsula, king George island (isla 25 mayo), NW antarctic peninsula. Front. Earth Sci. 10, 1073075. https://doi.org/10.3389/feart.2022.1073075.

Hillenbrand, C.-D., Larter, R.D., Dowdeswell, J.A., Ehrmann, W., Ó Cofaigh, C., Benetti, S., Graham, A.G.C., Grobe, H., 2010. The sedimentary legacy of a palaeo-ice stream on the shelf of the southern Bellingshausen Sea: clues to West Antarctic glacial history during the Late Quaternary. Quat. Sci. Rev. 29, 2741–2763. https://doi.org/10.1016/j.quascirev.2010.06.028.

Hrbáček, F., Oliva, M., Ruiz-Fernández, J., Kňažková, M., de Pablo, M.A., 2020. Modelling ground thermal regime in bordering (dis) continuous permafrost environments. Env. Res. 181, 108901. https://doi.org/10.1016/j.envres.2019.108901.

Hrbáček, F., Oliva, M., Abramov, A., de Pablo, M.A., Ramos, M., Vieira, G., Goyanes, G., Hansen, C., O'Neill, T., Lacelle, D., Ponti, S., Guglielmin, M., Pastirikova, L., Schaefer, C., Francellino, M., 2023. Active layer and permafrost thermal regimes in the ice-free areas of Antarctica. Earth Sci. Rev. 242, 104458. https://doi.org/10.1016/j.earscirev.2023.104458.

Ingólfsson, Ó., Hjort, C., Berkman, P.A., Björck, S., Colhoun, E., Goodwin, I.D., Hall, B., Hirakawa, K., Melles, M., Möller, P., Prentice, M.L., 1998. Antarctic glacial history since the Last Glacial Maximum: an overview of the record on land. Antarct. Sci. 10, 326–344. https://doi.org/10.1017/S095410209800039X.

John, B.S., Sugden, D.E., 1972. Raised marine features and phases of glaciation in the South Shetland Islands. Brit. Antarct. Surv. B. 24, 45–111.

Johnson, J.S., Everest, J.D., Leat, P.T., Golledge, N.R., Rood, D.H., Stuart, F.M., 2012. The deglacial history of NW Alexander Island, Antarctica, from surface exposure dating. Quat. Res. 77, 273–280. https://doi.org/10.1016/j.yqres.2011.11.012.

Kaplan, M.R., Strelin, J.A., Schaefer, J.M., Peltier, C., Martini, M.A., Flores, E., Winckler, G., Schwartz, R., 2020. Holocene glacier behavior around the northern Antarctic Peninsula and possible causes. Earth Planet Sci. Lett. 534, 116077. https://doi.org/10.1016/j.epsl.2020.116077.

Korschinek, G., Bergmaier, A., Faestermann, T., Gerstmann, U.C., Knie, K., Rugel, G., Wallner, A., Dillmann, I., Dollinger, G., von Gostomski, C.L., Kossert, K., Maiti, M., Poutivtsev, M., Remmert, A., 2010. A new value for the half-life of ^{10}Be by Heavy-Ion Elastic Recoil Detection and liquid scintillation counting. Nucl. Instrum. Methods Phys. Res. B 268, 187–191. https://doi.org/10.1016/j.nimb.2009.09.020.

Li, Y., 2018. Determining topographic shielding from digital elevation models for cosmogenic nuclide analysis: a GIS model for discrete sample sites. J. Mt. Sci. 15, 939–947. https://doi.org/10.1007/s11629-018-4895-4.

Lifton, N., Sato, T., Dunai, T.J., 2014. Scaling in situ cosmogenic nuclide production rates using analytical approximations to atmospheric cosmic-ray fluxes. Earth Planet Sci. Lett. 386, 149–160. https://doi.org/10.1016/J.EPSL.2013.10.052.

López-Martínez, J., Serrano, E., Schmid, T., Mink, S., Linés, C., 2012. Periglacial processes and landforms in the South Shetland islands (northern antarctic peninsula region). Geomorphology 155–156, 62–79. https://doi.org/10.1016/j.geomorph.2011.12.018.

McCarthy, D.P., Luckman, B.H., 1993. Estimating ecesis for tree-ring dating of moraines: a comparative study from the Canadian cordillera. Arct Antarct Alp Res 25, 63–68. https://doi.org/10.2307/1551482.

Merchel, S., Arnold, M., Aumaître, G., Benedetti, L., Bourlès, D.L., Braucher, R., Alfimov, V., Freeman, S.P.H.T., Steier, P., Wallner, A., 2008. Towards more precise ^{10}Be and ^{36}Cl data from measurements at the 10-14 level: influence of sample preparation. Nucl. Instrum. Methods Phys. Res. B 266, 4921–4926. https://doi.org/10.1016/j.nimb.2008.07.031.

Merchel, S., Herpers, U., 1999. An update on radiochemical separation techniques for the determination of long-lived radionuclides via accelerator mass spectrometry. Radiochim. Acta 84, 215–219. https://doi.org/10.1524/ract.1999.84.4.215.

Milliken, K.T., Anderson, J.B., Wellner, J.S., Bohaty, S.M., Manley, P.L., 2009. High-resolution Holocene climate record from Maxwell bay, South Shetland islands, Antarctica. Bull. Geol. Soc. Am. 121 (1), 1711–1725. https://doi.org/10.1130/B26478.

Molina, C., Navarro, F.J., Calvet, J., García-Sellés, D., Lapazaran, J.J., 2007. Hurd Peninsula glaciers, Livingston Island, Antarctica, as indicators of regional warming: ice-volume changes during the period 1956-2000. Ann. Glaciol. 46, 43–49. https://doi.org/10.3189/172756407782871765.

Navarro, F.J., Jonsell, U.Y., Corcuera, M.I., Martín-Español, A., 2013. Decelerated mass loss of Hurd and Johnsons glaciers, Livingston island, antarctic peninsula. J. Glaciol. 59, 115–128. https://doi.org/10.3189/2013JoG12J144.

Navas, A., Oliva, M., Ruiz-Fernández, J., Gaspar, L., Quijano, L., Lizaga, I., 2017. Radionuclides and soil properties as indicators of glacier retreat in a recently deglaciated permafrost environment of the Maritime Antarctica. Sci. Total Environ. 609, 192–204. https://doi.org/10.1016/j.scitotenv.2017.07.115.

Nývlt, D., Glasser, N.F., Oliva, M., Roberts, S.J., Roman, M., 2020. Tracing the deglaciation since the last glacial maximum. In: Oliva, M., Ruiz-Fernández, J. (Eds.), Past Antarctica, pp. 89–108.

Ó Cofaigh, C., Davies, B.J., Livingstone, S.J., Smith, J.A., Johnson, J.S., Hocking, E.P., Hodgson, D.A., Anderson, J.B., Bentley, M.J., Canals, M., Domack, E., Dowdeswell, J. A., Evans, J., Glasser, N.F., Hillenbrand, C.D., Larter, R.D., Roberts, S.J., Simms, A. R., 2014. Reconstruction of ice-sheet changes in the antarctic peninsula since the last glacial maximum. Quat. Sci. Rev. 100, 87–110. https://doi.org/10.1016/j.quascirev.2014.06.023.

Oliva, M., Antoniades, D., Giralt, S., Granados, I., Pla-Rabes, S., Toro, M., Liu, E.J., Sanjurjo, J., Vieira, G., 2016a. The Holocene deglaciation of the Byers Peninsula (Livingston Island, Antarctica) based on the dating of lake sedimentary records. Geomorphology 261, 89–102. https://doi.org/10.1016/j.geomorph.2016.02.029.

Oliva, M., Antoniades, D., Giralt, S., Granados, I., Pla-Rabes, S., Toro, M., Sanjurjo, J., 2016b. La deglaciación de las áreas libres de hielo de las islas Shetland del Sur (Antártida): Ejemplos de Byers (Livingston) y Barton (King George). Cuaternario Geomorfol. 30, 105–118. https://doi.org/10.17735/cyg.v30i1-2.48665.

Oliva, M., Antoniades, D., Serrano, E., Giralt, S., Liu, E.J., Granados, I., Pla-Rabes, S., Toro, M., Hong, S.G., 2019a. The deglaciation of Barton peninsula (king George island, South Shetland islands, Antarctica) based on geomorphological evidence and lacustrine records. Polar Rec. 55, 177–188.

Oliva, M., Navarro, F., Hrbáček, F., Hernández, A., Nývlt, D., Pereira, P., Ruiz-Fernández, J., Trigo, R., 2017. Recent regional climate cooling on the Antarctic Peninsula and associated impacts on the cryosphere. Sci. Total Environ. 580, 210–223. https://doi.org/10.1016/j.scitotenv.2016.12.030.

Oliva, M., Palacios, D., Fernández-Fernández, J.M., Fernandes, M., Schimmelpfennig, I., Vieira, G., Antoniades, D., Pérez-Alberti, A., García-Oteyza, J., Team, A., 2023. Holocene deglaciation of the northern Fildes peninsula, king George island, Antarctica. Land Degrad. Dev. 34, 3973–3990.

Oliva, M., Ruiz-Fernández, J., Palacios, D., Fernández-Fernández, J.M., Schimmelpfennig, I., González-Díaz, B., ASTER Team, 2019b. Nunataks as keys to understanding the deglaciation process of ice-free environments in Antarctica. In: Abstracts of the VII Iberian Conference of the International Permafrost Association, p. 3.

Osmanoglu, B., Navarro, F.J., Hock, R., Braun, M., Corcuera, M.I., 2014. Surface velocity and mass balance of Livingston Island ice cap, Antarctica. Cryosphere 8, 1807–1823. https://doi.org/10.5194/tc-8-1807-2014.

Palacios, D., Ruiz-Fernández, J., Oliva, M., Andrés, N., Fernández-Fernández, J.M., Schimmelpfennig, I., Leanni, L., González-Díaz, B., 2020. Timing of formation of neoglacial landforms in the South Shetland islands (antarctic peninsula): regional and global implications. Quat. Sci. Rev. 234, 106248. https://doi.org/10.1016/j.quascirev.2020.106248.

Porter, S., 2001. Onset of neoglaciation in the southern hemisphere. J. Quat. Sci. 15 (4), 395–408.

Roberts, S.J., Monien, P., Foster, L.C., Loftfield, J., Hocking, E.P., Schnetger, B., Pearson, E.J., Juggins, S., Fretwell, P., Ireland, L., Ochyra, R., Haworth, A.R., Allen, C.S., Moreton, S.G., Davies, S.J., Bentley, M.J., Hodgson, D.A., 2017. Past penguin colony responses to explosive volcanism on the Antarctic Peninsula. Nat. Commun. 8, 14914. https://doi.org/10.1038/ncomms14914.

Raggio, J., Green, T.G.A., Pintado, A., Sancho, L.G., 2018. Photosynthetic rate and thallus size are not related in alpine yellow-green Rhizocarpon crustose lichens: implications for lichenometry and growth. Geomorphology 318, 348–353.

Ruiz-Fernández, J., Oliva, M., 2016. Relative palaeoenvironmental adjustments following deglaciation of the Byers peninsula (livingstone island, Antarctica). Arct Antarct Alp Res 48 (2), 345–359. https://doi.org/10.1657/AAAR0015-014.

Ruiz-Fernández, J., Oliva, M., Nývlt, D., Cannone, N., García-Hernández, C., Guglielmin, M., Hrbáček, F., Roman, M., Fernández, S., López-Martínez, J., Antoniades, D., 2019. Patterns of spatio-temporal paraglacial response in the

Antarctic Peninsula region and associated ecological implications. Earth Sci. Rev. 192, 379–402. https://doi.org/10.1016/j.earscirev.2019.03.014.
Sancho, L.G., Palacios, D., Green, T.A., Vivas, M., Pintado, A., 2011. Extreme high lichen growth rates detected in recently deglaciated areas in Tierra del Fuego. Polar Biol. 34, 813–822.
Sancho, L.G., Pintado, A., Navarro, F., Ramos, M., De Pablo, M.A., Blanquer, J.M., Raggio, J., Valladares, F., Green, T.G.A., 2017. Recent warming and cooling in the antarctic peninsula region has rapid and large effects on lichen vegetation. Sci. Rep. 7, 5689. https://doi.org/10.1038/s41598-017-05989-4.
Seong, Y.B., Owen, L.A., Lim, H.S., Yoon, H. Il, Kim, Y., Lee, Y. Il, Caffee, M.W., 2009. Rate of late quaternary ice-cap thinning on king George island, South Shetland islands, west Antarctica defined by cosmogenic 36Cl surface exposure dating. Boreas 38, 207–213. https://doi.org/10.1111/j.1502-3885.2008.00069.x.
Simms, A.R., Bentley, M.J., Simkins, L.M., Zurbuchen, J., Reynolds, L.C., Dewitt, R., Thomas, E.R., 2021. Evidence for a "Little Ice Age " glacial advance within the Antarctic Peninsula e Examples from glacially-overrun raised beaches. Quat. Sci. Rev. 271, 107195. https://doi.org/10.1016/j.quascirev.2021.107195.
Simms, A.R., Milliken, K.T., Anderson, J.B., Wellner, J.S., 2011. The marine record of deglaciation of the South Shetland islands, Antarctica since the last glacial maximum. Quat. Sci. Rev. 30, 1583–1601. https://doi.org/10.1016/j.quascirev.2011.03.018.
Small, D., Bentley, M.J., Jones, R.S., Pittard, M.L., Whitehouse, P.L., 2019. Antarctic ice sheet palaeo-thinning rates from vertical transects of cosmogenic exposure ages. Quat. Sci. Rev. 206, 65–80. https://doi.org/10.1016/j.quascirev.2018.12.024.
Smellie, J.L., Liesa, M., Muñoz, J.A., Sàbat, F., Pallàs, R., 1995. Lithostratigraphy of volcanic and sedimentary sequences in central Livingston island, South Shetland islands. Antarct. Sci. 7, 99–113. https://doi.org/10.1017/S0954102095000137.
Smith, J.A., Hillenbrand, C., Kuhn, G., Larter, R.D., Graham, A.G.C., Ehrmann, W., Moreton, S.G., Forwick, M., 2011. Deglacial history of the west antarctic ice sheet in the western amundsen sea embayment. Quat. Sci. Rev. 30, 488–505. https://doi.org/10.1016/j.quascirev.2010.11.020.
Stone, J.O., 2000. Air pressure and cosmogenic isotope production. J. Geophys. Res. Solid Earth 105, 23753–23759. https://doi.org/10.1029/2000JB900181.
Tatur, A., Valle, R.D.E.L., Martínez-Macchiavello, J.C., Tatur, A., Servant-Vildary, S., Del Valle, R., 1996. Holocene environmental change in a marine-estuarine-lacustrine sediment sequence, king George island, South Shetland islands. Antarct. Sci. 8, 313–322. https://doi.org/10.1017/S095410209600048X.
Taylor, J.R., 1997. An introduction to error analysis. The Study of Uncertainties in Physical Measurements. University Science Books, Sausalito, USA.
Toro, M., Granados, I., Pla, S., Giralt, S., Antoniades, D., Galán, L., Cortizas, A.M., Lim, H. S., Appleby, P.G., 2013. Chronostratigraphy of the sedimentary record of limnopolar lake, Byers peninsula, Livingston island, Antarctica. Antarct. Sci. 25, 198–212. https://doi.org/10.1017/S0954102012000788.
Turner, J., Colwell, S.R., Marshall, G.J., Lachlan-Cope, T.A., Carleton, A.M., Jones, P.D., Lagun, V., Reid, P.A., Iagovkina, S., 2005. Antarctic climate change during the last 50 years. Int. J. Climatol. 25, 279–294. https://doi.org/10.1002/joc.1130.
Vieira, G., Bockheim, J., Guglielmin, M., Balks, M., Abramov, A.A., Boelhouwers, J., Cannone, N., Ganzert, L., Gilichinsky, D.A., Goryachkin, S., López-Martínez, J., Meiklejohn, I., Raffi, R., Ramos, M., Schaefer, C., Serrano, E., Simas, F., Sletten, R., Wagner, D., 2010. Thermal state of permafrost and active-layer monitoring in the antarctic: advances during the international polar year 2007-2009. Permafr. Periglac. Process. 21, 182–197. https://doi.org/10.1002/ppp.685.
Watcham, E.P., Bentley, M.J., Hodgson, D.A., Roberts, S.J., Fretwell, P.T., Lloyd, J.M., Larter, R.D., Whitehouse, P.L., Leng, M.J., Monien, P., Moreton, S.G., 2011. A new Holocene relative sea level curve for the South Shetland Islands, Antarctica. Quat. Sci. Rev. 30, 3152–3170. https://doi.org/10.1016/j.quascirev.2011.07.021.
Yoon, H. Il, Han, M.W., Park, B.K., Oh, J.K., Chang, S.K., 1997. Glaciomarine sedimentation and palaeo-glacial setting of Maxwell bay and its tributary embayment, marian cove, South Shetland islands, west Antarctica. Mar. Geol. 140, 265–282. https://doi.org/10.1016/S0025-3227(97)00028-5.
Young, E., Briner, J.P., Miller, G.H., Lesnek, A.J., Crump, S.E., Thomas, E.K., Pendleton, S.L., Cuzzone, J., Lamp, J., Zimmerman, S., Caffee, M., Schaefer, J.M., 2020. Deglaciation of the Greenland and Laurentide ice sheets interrupted by glacier advance during abrupt coolings. Quat. Sci. Rev. 229, 106091. https://doi.org/10.1016/j.quascirev.2019.106091.